Investigation of the nature and stability of the Martian seasonal water cycle with a general circulation model

Mark I. Richardson

Division of Geological and Planetary Sciences, California Institute of Technology, Pasadena, California, USA

R. John Wilson

Geophysical Fluid Dynamics Laboratory, National Oceanic and Atmospheric Administration, Princeton, New Jersey, USA

[1] We describe the first use of a general circulation model to study the Martian water cycle. Water is treated as a passive tracer, except for ice-albedo coupling. The model is used to assess which mechanisms and water reservoirs are critical to the seasonal evolution of water and specifically the attainment of an interannually repeatable steady state. The model comes to a reasonable steady state with active surface ice and atmospheric vapor and ice reservoirs. A regolith is not necessary. The mechanism of equilibration results from independent parameters controlling the transport of water between the northern polar and the extratropical atmospheres at different seasons. Water export from the northern summer pole results from weak mixing across a strong vapor gradient, dependent upon northern cap temperatures. Import at other seasons depends on stronger mixing and weak vapor gradients, which are history dependent. Equilibration is achieved when the fluxes balance, minus a small net loss to the south. We find that with a southern residual CO_2 cap, the water cycle cannot be completely closed. We conclude that the northern summer cap temperature determines the bulk humidity of the atmosphere, all else being equal. We proceed to show that a water cap exposed in southern summer would be unstable with respect to the north for dynamical as well as thermal reasons. At high obliquity (45°), much higher vapor abundances result in more widespread surface ice with seasonal ice caps overlapping in the equinoctial subtropics, producing year-round stability of water ice just north of the equator.   *INDEX TERMS:* 5445 Planetology: Solid Surface Planets: Meteorology (3346); 5462 Planetology: Solid Surface Planets: Polar regions; 5409 Planetology: Solid Surface Planets: Atmospheres—structure and dynamics; 6225 Planetology: Solar System Objects: Mars; *KEYWORDS:* Mars, water, climate, atmosphere, ice, cap

1. Introduction

[2] Mars currently possess an active hydrologic cycle. Spacecraft and ground-based observations show a strong seasonal cycle of water between surface deposits of ice, atmospheric vapor, and atmospheric water ice [*Jakosky and Haberle*, 1992]. It is also known from laboratory experiments that water should adsorb to grains and pore walls of the subsurface and that exchange between adsorbed and other water phases should be significant. The liquid phase is believed absent for present climatic conditions [*Jakosky*, 1985].

[3] There have been a number of attempts to develop predictive models of the Martian water cycle [e.g., *Davies*, 1981; *Jakosky*, 1983b; *Houben et al.*, 1997] since the acquisition of the milestone Mars Atmospheric Water Detector (MAWD) water vapor data set in the late-1970s [*Farmer et al.*, 1977; *Jakosky and Farmer*, 1982]. Such modeling serves two purposes. First, it allows us to see whether we can understand the data set in physical terms. Ultimately, this becomes an exercise in determining the relative importance of various processes and the degree of precision with which they need to be represented. The second, but closely related reason for developing physical models, is the desire to use these models to conduct "what if?" experiments. This is particularly intriguing for Mars in that there has likely been great variability of climate, even after the demise of a putative early, "warm, wet" climate. The geological evidence for this takes the form of the polar layered terrains, outflow channels, suspected glacial features, and putative oceanic shore lines [*Baker et al.*, 1991; *Kieffer and Zent*, 1992]. As all of these phenomena include water as a primary agent, the evolution of the water cycle as a function of time and varied forcing is of great interest for the study of Mars paleoclimate.

[4] In this report, we describe the first use of a full Mars general circulation model (GCM) to study the Martian water cycle. The GCM provides a framework within which the various water cycle processes can interact to evolve distributions of vapor, ice, and adsorbate. Importantly, the model calculates transport fluxes self-consistently, once provided

with radiative forcing (the diurnal and seasonal cycles of sunlight), a description of thermal and radiative properties (atmospheric heat capacity, surface albedo and thermal inertia, aerosol optical properties, etc.), and boundary conditions (e.g., topography and surface roughness at the lower boundary). The quality of the resulting transport is gauged indirectly, by comparing predicted and observed atmospheric temperature and pressure fields, and directly, by comparing model and observed distributions of dust. Mars GCMs now compare reasonably well with remotely sensed data from Mariner 9 and Viking [*Haberle et al.*, 1993; *Barnes et al.*, 1993; *Wilson and Hamilton*, 1996; *Wilson*, 1997; *Forget et al.*, 1999]. They have also begun to make progress in understanding the higher temporal and spatial resolution data from Mars Global Surveyor (MGS) [e.g., *Wilson*, 2000]. Although significant work still remains to be done before we can have confidence in our quantitative understanding of the Martian circulation and climate system (significant knowledge gaps include the mechanisms responsible for the maintenance of the dust haze, the genesis and early evolution of dust storms, albedo variations in the polar ice deposits, and the importance of water ice clouds), global models have advanced to the point where exploration of system behavior, such as the water cycle, is viable. Indeed, to make progress in understanding the water cycle, global modeling must be used in conjunction with data, if only to highlight omissions or misrepresentations of significant processes or interactions. In addition, global models provide the best method of exploring system sensitivity to variations in forcing associated with rotation axis and orbital variations and injection or removal of greenhouse gases. Thus a significant motivation for this study is the belief that Mars GCMs should provide a powerful tool for investigation of Mars paleoclimate in the same way that the terrestrial GCMs have been applied to understand the evolution of climate on the Earth. In view of the longer-term goal of applying knowledge of the current cycle to issues of paleoclimate, we concentrate in this paper on examining the fundamental mechanisms controlling the Martian water)cycle, and specifically the stability of water ice deposits, the distribution of vapor, the partitioning of water between the atmosphere, surface, and subsurface, and the total amount of water present in the atmosphere.

1.1. Observations

[5] The primary motivator for models of the Martian water cycle is the global vapor data set provided by the Viking Orbiter MAWD instruments [*Farmer et al.*, 1977; *Jakosky and Farmer*, 1982]. Figure 1 shows MAWD zonal average vapor amounts for the first two Viking years. The dominant signal evident in the data is the accumulation of large amounts of vapor in the mid- to high-northern latitudes during northern summer. Sampling from the three Viking years show this signal to be robust, as do terrestrial observations [*Jakosky and Barker*, 1984; *Sprague et al.*, 1996] and more recently, analysis of MGS Thermal Emission Spectrometer (TES) data [*Smith*, 2002]. Southern summer is not associated with such a large accumulation in vapor at high southern latitudes, but vapor is underestimated during southern spring and summer owing to two large dust storms (their occurrence at $L_s = 210°$ and $L_s = 270°$ is evident by the sharp drops in vapor (L_s is the
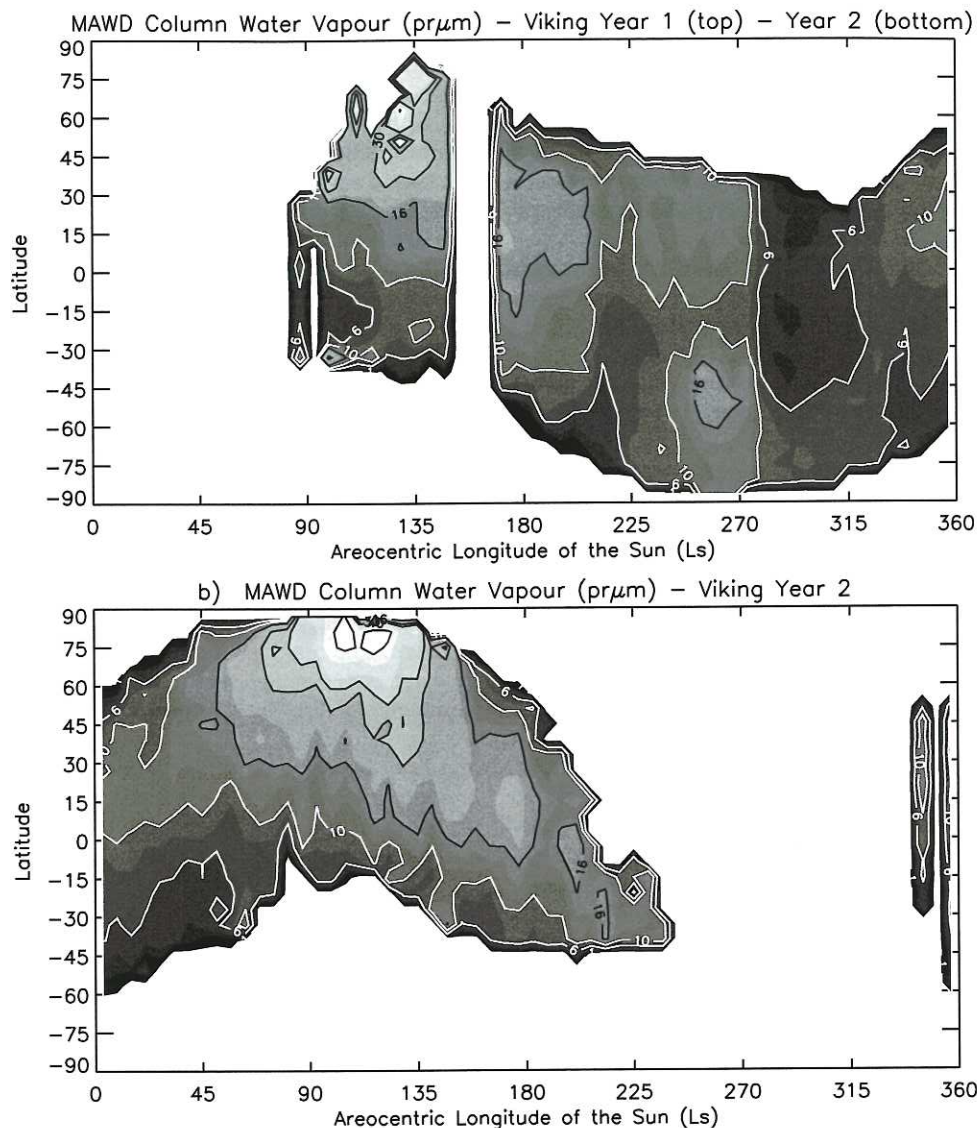
seasonal indicator for application to Mars (and many other planetary bodies); it is an angular measure, with $L_s = 0°$ defined as northern equinox, $L_s = 90°$ as northern summer solstice, etc.). As MAWD measured vapor by comparing the amount of reflected near-infrared sunlight inside and outside of vapor absorption lines in the 1.4-μm region, scattering by dust reduced the sampled path length and hence the total vapor column (this suggestion now appears to be supported by comparison with vapor measurements derived from TES data [*Smith*, 2002]). In any case, the MAWD data during clearer portions of southern spring and summer, TES data, and ground-based observations from other years, suggest that southern summer vapor amounts are generally far less (peak column values a factor of 3 or more smaller) than observed in the northern summer [*Jakosky and Farmer*, 1982; *Jakosky and Barker*, 1984; *Sprague et al.*, 1996].

[6] The use of the MAWD data as a standard with which to compare models is only sound if there is little interannual variability. While the MAWD data appear consistent with a repeatable cycle, ground-based observations suggest some modest variability [*Jakosky and Barker*, 1984; *Sprague et al.*, 1996; *Clancy et al.*, 2000]. Interannual comparison is, however, made difficult owing to potential biasing in longitude, the fact that although sensitive to topography, the MAWD data were retrieved long before accurate topographic data were available, and the fact that southern summer MAWD observations were significantly affected by high atmospheric dust amounts. Analysis of TES data [*Smith*, 2002] suggests a cycle of water vapor very similar to that observed by MAWD, especially when considering the differences in observational technique and retrieval approach. Certainly, TES data appear to reproduce all of the major features that can be seen in the MAWD data and confirm the elevated vapor amounts in the southern polar region and northern subtropics during southern summer (Figure 1). In any case, for the purposes of this article we will concentrate on trying to explain the physical processes responsible for a Martian water cycle like that observed by MAWD, with the understanding that not every year may be exactly alike.

1.2. Previous Water Cycle Models

[7] Three major questions result from the MAWD observations of the annual vapor cycle: (1) Why is the northern summer pole associated with higher vapor amounts than southern summer? (2) Given the observed preponderance of vapor during northern summer, can the water cycle be in a state of equilibrium or is there net north to south transfer of water? (3) What controls the global and annual average amount of water contained in the atmosphere? A trivial answer to the first question is that a permanent water ice cap is located in the north and not in the south, but why does not the south also have a permanent water ice cap? On a more systemic level, what processes are of dominant importance in producing the observed water cycle?

[8] Although it seems possible that the annual average, north-south vapor gradient suggested by MAWD may result from biases in that data set due to dust (this suggestion appears supported by recent comparisons with TES observations [*Smith*, 2002]), it has provided a major motivator for water cycle models. If accepted, the large, annual average, meridional vapor gradient suggests either that there is an

Figure 1. The latitudinal and seasonal distribution of water vapor in the Martian atmosphere, as observed by the Viking Mars Atmospheric Water Detector (MAWD) [*Farmer et al.*, 1977; *Jakosky and Farmer*, 1982]. The data have been zonally averaged and binned by 6° of latitude and 6° of L_s. The contour and color levels are on the same scale, with color intervals at 1, 2, 3, 4, 6, 8, 10, 12, 14, 16, 20, 30, 40, 50, 70, and 90 prμm, and contour levels at 1, 6, 10, 16, 30, 40, and 90 prμm. Data are shown for the first and second years of Viking observations; the third year of data being extremely sparse. The blue horizontal lines in Year 1 (top) roughly indicate the occurrence of two major dust storms that significantly degrade data quality. Despite the dust storms, note the appearance of two maxima in water vapor during southern summer (between the storms, $L_s = 250°-270°$), with one maxima in the high southern latitudes and one in the northern tropics. See color version of this figure at back of this issue.

equilibration mechanism acting to prevent water loss to the south or that water is in fact being transferred between the northern and southern polar regions. *Davies* [1981] produced the first model to frame water cycle equilibration question in terms of relative efficiencies of meridional water transport during the two solsticial periods. The model described atmospheric transport by downgradient diffusion with a spatially uniform coefficient. In addition, the model ignored regolith sites and used the MAWD data to prescribe the maximum amount of vapor the atmosphere could hold during northern summer. The major result was that a

MAWD-like distribution could be produced without net flow to the south if there were a large difference in atmospheric diffusivities between northern and southern summer. The physical mechanism for the asymmetry in diffusivities was ascribed to the hemispheric asymmetry in global dust storm activity. However, there were three main problems with the result. The required diffusion coefficient asymmetry was found to be large (roughly a factor of 50), probably unrealistically so. A model based on dust-storm enhancement of effective diffusivity is extremely sensitive to interannual variability in dust storm activity. However,

most importantly, the model lacked a "cold trap" at the southern pole to represent the permanent CO_2 ice cap.

[9] *Jakosky and Farmer* [1982] point out that a CO_2 ice cap cold trap means that some net loss to the south is unavoidable. (They went on to use the MAWD data to suggest that the maximum vapor loss in any given year is roughly 4×10^{14} g, compared to a globally integrated vapor content of the atmosphere of $1-2 \times 10^{15}$ g at any given instant. However, while this large value likely does overestimate true fluxes, it is not a true upper limit, as without knowledge of the spatial and temporal variability of transport fluxes one cannot strictly derive sublimation fluxes from instantaneous vapor amounts.) *Jakosky* [1983b] developed a model that differed from *Davies'* [1981] by the inclusion of a regolith reservoir and a CO_2 ice cap in the south and the elimination of the prescribed atmospheric holding capacity. Because of the cold trap, the model resulted in a nonequilibrium water cycle with loss to the south. Loss rates varied between 1.4 and 4.1×10^{14} g/yr, depending mainly on the vigor of atmospheric mixing. Interestingly, *Jakosky* [1983b] was able to reproduce a MAWD-like water cycle with a temporally uniform diffusivity. This contrasts with the expectation that uniform diffusivity should lead to roughly globally uniform vapor, on the annual average, and the results of *Davies* [1981]. We will discuss this aspect of the *Jakosky* [1983b] model further in section 3. The *Jakosky* [1983a, 1983b] study is primarily of importance as it provided the first integrated model of the Mars water cycle and demonstrated the importance of the components used in subsequent global water cycle models: the residual and seasonal water ice caps, and regolith adsorbate. *Jakosky's* [1983b] conclusion is particularly important for those interested in the physical basis of the water cycle and its likely response to varied forcing. *Jakosky*, [1983b, p. 38] stated that the polar caps control atmospheric vapor amounts in response to insolation and that the regolith water amount then varies so as to come into equilibrium with the atmosphere: "Thus, the polar caps dominate control of the entire process." We will ultimately arrive at this same high-level conclusion.

[10] *James* [1985] returned to the problem of how an annual average, latitudinal gradient in water vapor can be maintained. If the CO_2 ice cap cold trap is assumed to represent a small sink for water (compared with the total amount transported between the hemispheres) each year, then some mechanism must function to return water to the north more effectively than it is transported to the south in northern summer. This is fundamentally the same problem addressed by *Davies* [1981], except that it is acknowledged that some amount of net transfer must take place: the quest is now for a quasi-equilibrium state, rather than a true equilibrium. *James* [1985] recognized that the CO_2 flow has an inherent seasonal asymmetry due to the fact that more of the atmosphere freezes out in southern winter than in northern winter. Hence the net south to north flow in southern spring is greater than the reverse flow in northern spring. The ability of the seasonal flow to produce an asymmetry in the global average, latitudinal vapor distribution was demonstrated using a model of the seasonal condensation flow combined with a diffusion model of the kind used by *Davies* [1981] and *Jakosky* [1983b], without the imposed saturation condition of the former or

the regolith of the latter. Another suggestion as to the origin of the seasonal asymmetry has been provided by *Clancy et al.* [1996], who pointed out the difference in saturation levels between northern and southern summer. The cooler northern summer has the lower level, and it was suggested that this limitation on vertical spreading limits the degree to which vapor can be transported south. This mechanism is examined by *Richardson et al.*, [2002]. Its viability depends on the relationship between saturation level and the vertical structure of circulation patterns and on the ratio of sedimentation rates and lateral transport rates.

[11] The most comprehensive study of the water cycle to date was performed by *Houben et al.*, [1997, hereinafter referred to as H97] using a simplified, 3-D climate model. Akin with the *Jakosky* [1983b] model, H97 found a net loss of water to the south (roughly 2.5×10^{14} g/yr). However, unlike *Jakosky* [1983b], H97 were not able to maintain an annual average, latitudinal vapor gradient without an active regolith. Importantly, from a mechanistic standpoint, H97 found that the atmosphere would "flood" with vapor, resulting in large perennial ice deposits if the regolith were inactive. The regolith in the H97 model acts to staunch the flow of water to the southern hemisphere during northern summer, and therefore helps "trap" the water in the north. As we will discuss in the main body of this article, we do not find that the atmosphere would flood with water in the absence of the regolith. Indeed, it now appears that the flooding in the H97 model results from an error in those calculations (H. Houben, personal communication, 1999). We will have occasion to describe the H97 model and the results flowing from it in more detail as we contrast that work with the present study. Thus we leave further discussion of the H97 model to later sections.

1.3. Organization

[12] In section 2, we describe the model used in this study, a Mars-adapted version of the Geophysical Fluid Dynamics Laboratory (GFDL) "Skyhi" GCM. We describe in outline the general processes contained in the model, and proceed to discuss the water processes in more detail. In section 3, we describe and discuss simulations in which the regolith is inactive. These simulations are designed to provide insight into the basic mechanisms of a simplified water cycle, involving only vapor and ice reservoirs. We specifically examine the processes that drive the model toward equilibrium, or more precisely, steady state. In the process the simulations provide a test of the H97 finding that the atmosphere would flood without the action of the regolith. They also provide a test of the conclusions derived from a 2-D model by *Haberle and Jakosky* [1990] that water cannot be effectively moved from the northern polar regions in summer. On the contrary, we find that in the full 3-D model one does not need to invoke regolith sources to explain water vapor that accrues in the tropics and mid-latitudes and that the model quickly develops interhemispheric exchange. In section 4, we discuss an experiment in which the CO_2 condensation flow is eliminated. Section 2 describes a simulation in which an active regolith is incorporated. In combination with the results of section 3, these simulations suggest a role for the regolith significantly less important than that postulated by H97 and by *Haberle and Jakosky* [1990]. The next two sections provide an initial

foray into Martian paleoclimate simulation. In section 6, we explore the stability of a hypothetical southern residual water ice cap with respect to the water ice cap at the northern pole. We impose southern cap ice properties such that the southern summer cap peak temperatures are cooler than those of the northern cap. This is done so as to provide a sublimation flux bias favoring southern cap stability. The question being addressed in this section is whether there exists a dynamical bias that favors stability of a northern, rather than a southern residual water ice cap. In section 7, we explore the model water cycle that would result if the planetary obliquity were changed from 25° to 45°. The simulations suggest much more extensive seasonal water ice deposits than at present, resulting in the effective year-round stability of surface water ice in the northern tropics. We summarize this work in section 8.

2. Model Description

[13] The model used in this study is the GFDL Mars GCM. This model is based upon the GFDL troposphere-stratosphere-mesosphere Skyhi GCM and has been adapted to Mars through the modification of physical processes and constants. Except where stated, the model used for the experiments discussed in this paper is as described by *Wilson and Hamilton* [1996], *Wilson* [1997], and *Wilson and Richardson* [2000]. Modifications include the use of Mars Orbiter Laser Altimeter (MOLA) topography [*Smith et al.*, 1999], the inclusion of polar albedo and thermal inertia data [*Vasavada*, 2000] to complete the global surface maps, and the processes that constitute the water cycle. In the following paragraphs, we briefly review the GFDL Mars GCM elements already described in previous papers and then proceed to a more thorough description of the water cycle processes.

2.1. General Model Description

[14] The GCM solves the primitive equations of atmospheric motion [e.g., *Holton*, 1992] at a finite number of discrete points so as to represent the global atmosphere. The model resolution can be varied. Typical resolutions include 5° by 6° (latitude by longitude) and 3° by 3.6° and the use of 20 or 40 vertical levels between the surface and roughly 85 km [see *Wilson and Hamilton*, 1996]. The lowest model level is typically a few hundred meters ($\sim$250 m) above the surface.

[15] Radiative heating associated with dust and with CO_2 provide the energetic drive for the modeled circulation. In the visible we employ the *Houghton* [1963] scheme (as implemented by *Burk* [1976]) for heating due to absorption in the near-infrared CO_2 bands, and model of *Briegleb* [1992] for heating due to dust absorption across the visible. The dust optical properties of *Clancy and Lee* [1991] are used. In the infrared we use the *Goody and Belton* [1967] formulation for heating/cooling in the CO_2 15-μm band, and the *Haberle et al.* [1982] model for heating and cooling by atmospheric dust. A more recent version of the radiation code treats scattering and absorption in both the visible and infrared. For reasons of heritage and consistency across the numerous and lengthy simulations described in this paper, we do not use the most recent version of the radiation code.

[16] Momentum and heat are mixed between the surface and atmosphere using a Monin-Obukhov surface drag model [e.g., *Stull*, 1988]. Above the surface layer, mixing is diffusive, with a Richardson number-dependent coefficient. In most cases, surface temperatures are computed based on net downward radiative fluxes, flux of sensible heat, CO_2 condensation/sublimation, and heat fluxes associated with heat diffusion within the regolith. A 12-layer subsurface heat diffusion model is used to calculate the latter term. When CO_2 ice is present on the surface, the surface temperature is held at the CO_2 condensation point.

[17] The Mars GCM includes a full CO_2 cycle and dynamically and radiatively active dust. For CO_2 the gas is allowed to condense on the surface so as to maintain energy balance when atmospheric temperatures reach the condensation point. Any CO_2 condensing in the atmosphere falls immediately to the surface. The resulting roughly 25% annual cycle of atmospheric pressure is in good agreement with observations. The model does not retain a permanent CO_2 ice cap at the southern pole (i.e., CO_2 ice completely sublimes) since the albedo of CO_2 ice is held constant. Instead, ground temperatures at the 87.5°S grid points are held constant at 148 K in order to simulate the effects of a residual cap. Dust is injected in the lowest atmospheric level at a temporally constant, prescribed rate. From the lowest level, transport occurs owing to the large-scale winds, subgrid-scale diffusion, and gravitational settling. The model quickly evolves a nearly steady state global distribution of dust (a variation of global dust loading is generated spontaneously by the model over seasonal timescales, roughly consistent with observations). Two particle sizes are used in these simulations (corresponding to 0.6- and 2.5-μm radii). The distribution of dust within a column is used as an input to the radiation code in order to calculate visible and infrared heating rates. Again, a more recent version of the model treats six dust particle sizes. The dust injection scheme and the evolving behavior of atmospheric dust are discussed in more detail by *Wilson and Hamilton* [1996].

[18] The model is begun in the simulations discussed in this paper from a fully spun-up initial condition; thus the details of initialization refer only to water. Specifically, most of the initial condition files used in this study derive from simulations in which the CO_2 cycle has been adjusted to match the Viking Lander pressure cycles, and the air temperatures to match microwave and Mars Global Surveyor Thermal Emission Spectrometer observations. In the case of pressure this involves varying the total atmospheric mass until the correct cycle naturally evolves. In the case of temperature, it involves varying the dust injection rate at the surface. Any deviation from these initial conditions is noted in the text.

2.2. Water Cycle Processes

[19] The transport of water vapor and water ice within the atmosphere takes advantage of the built-in tracer advection capability of the GCM dynamical core [see *Hamilton et al.*, 1995, and references therein]. Akin with the treatment of atmospheric dust, water ice and vapor are carried within the model as three-dimensional fields. The amount of tracer in any given grid box (in units of mass mixing ratio) is determined by a continuity equation for that tracer, which

includes source and sink terms, advection by the model-resolved winds, and diffusion. For water ice, gravitational settling is also treated, using the Stokes-Cunningham relation for spherical particles [e.g., *Conrath*, 1975].

[20] Condensation of water, both in the atmosphere and on the surface is governed by the saturation vapor pressure determined via the equation:

$$P_{sat} = 6.11 \times \exp\left[22.5 \times \left(1. - \frac{273.16}{T}\right)\right],$$

where P_{sat} is the saturation vapor pressure in Pascals, and T is the temperature in kelvin.. This formulation agrees well with standard high- and low-temperature approximations [*Goff and Gratch*, 1946; *Bar-Nun et al.*, 1985]. If more than 3 prμm (precipitable micron, or 10^{-4} g cm^{-2}) of water ice accumulates on the surface, the albedo of that grid box is set to 0.4. Latent heating due to water condensation and sublimation is ignored.

[21] The treatment of upward fluxes of vapor from a surface water ice deposit is derived from *Ingersoll* [1970] (we use unmodified (1) and (2) of *Haberle and Jakosky* [1990]). This scheme calculates the flux based on the vapor pressure difference between that just above the ice and in the lowest model level, on the wind speed above the ground, and on the mean molecular mass gradient associated with having lighter water molecules underlying those of CO_2. The downward flux across the surface layer is calculated from the vapor pressure difference between the lowest model level and the condensation point pressure appropriate for the layer temperature. Sufficient ice is converted in each time step so that the layer never becomes supersaturated. In a very limited number of cases, as mentioned in the text, a linear time constant is applied to removal of supersaturated vapor, so as to mimic the effects of a stable boundary layer.

[22] The northern polar cap must be prescribed in the model. Given the 5° latitudinal resolution, we chose to impose the water ice cap (as an inexhaustibly large reservoir) at the two most northerly grid points (87.5°N and 82.5°N), corresponding to a circular cap 10° in diameter, centered on the northern pole. This results in an unrealistically large cap but is the best approximation that can be made. Simulations with higher-resolution GCMs and/or with mesoscale models focused on the pole should be undertaken in the future to assess the impact of this assumption. In any case, it is likely that the current GCM overestimates northern cap supply of vapor given the excessive cap area.

[23] Water condensation in the atmosphere is described with a simple parameterization that converts any supersaturated vapor into water ice particles of a prescribed size (2 μm). Conversely, if ice is present in a subsaturated grid box, sufficient ice is sublimed such that the grid box is just saturated. If insufficient ice is available to reach saturation, all the ice is sublimed. In both cases the mass is added to the vapor budget. Conversion of supersaturated vapor to ice is instantaneous, except in a few simulations (as indicated in the text) where a linear time constant is used to retard condensation in an attempt to capture aspects of microphysics that allow for supersaturation. In the former case, the phase change process is symmetric about the condensation point, while in the latter an activation energy barrier to

condensation is present (associated with the excess partial pressure necessary to drive nucleation and growth on a surface of high curvature), but no such barrier is physically plausible for sublimation. No ice is allowed in the lowest model level (any supersaturated vapor is converted to surface ice; this is equivalent to assuming that condensates formed in the lowest level precipitate to the surface on the timescale of one model time step). In these calculations, latent heating due to condensation and sublimation of water ice is ignored, as are the radiative effects of clouds. It is easy to show that the latent heating effect of water phase change is small and that the fundamental reason for this is the very low abundance of water in the atmosphere. Assuming that all the water vapor in even the most moist Martian air column condenses, it is sufficient to raise temperatures by only roughly a tenth of a kelvin [*Zurek et al.*, 1992]. Alternatively, the difference between the moist and dry adiabats on Mars is only ~0.1%. The assumption that clouds are not radiatively important is far more suspect, and one that should be revisited in future work. In addition, potential interactions between dust and water condensation also remain untreated in this work.

[24] The only interaction between water and the rest of the Mars GCM is through the ability of surface water ice to modify the surface albedo (we vary the water ice albedo in different simulations). However, modeled water ice generally forms in association with the CO_2 seasonal ice cap, and in that case we allow the CO_2 ice albedo (0.6) to dominate. In reality, water likely influences the global climate system in other ways, for example, through interactions between dust and water [*Clancy*, 1996]. These interactions are beyond the scope of this paper and will be examined in later studies with this model.

3. Interannual Water Cycle Evolution Without Active Regolith

[25] The Martian water cycle likely results from the interaction of a number of processes, each of which is spatially and temporally variable. Some benefit in understanding the interaction of these processes is afforded by initially examining a subset of them. Since the regolith is both the least well-constrained component of the system and the one with the longest characteristic timescale for exchange, initially eliminating the regolith allows both for faster equilibration of the cycle and reduction in complexity. Additionally, one of the significant results from the H97 study was the finding that the Martian atmosphere would flood with water without a regolith. On the other hand, *Haberle and Jakosky* [1990] claim that the northern summer polar circulation is sufficiently weak that without a regolith source, the Martian atmosphere would be much more dry than observed. Thus, in this section, we describe simulations with a full GCM undertaken to assess whether the water cycle would equilibrate without regolith adsorbate action, and if so, at what global vapor mass and how quickly. Equilibration is defined here as the establishment of a repeatable water cycle with no effective net interannual drift in the global budgets of vapor, ice, or cloud. We conduct a number of simulations with different initial global vapor inventories and different temperature structures. Important characteristics of these runs are provided

Table 1. Names and Pertinent Characteristics of Interannual Simulations Without Active Regolith Employed in Section 3 to Elucidate Equilibration Mechanisms

Simulation	Air Temperatures	Peak Cap Temperatures	Initial Vapor
Viking (VS)	fit to microwave, "corrected" IRTM T15, and TES	~2 K cooler	1.25×10^{15} g
Equilibrium (ES)	cooler than observed (by ~5 K at $L_s = 90°$)	~5 K warmer	None
Warm, wet (WW)	warmer than observed (by ~8 K at $L_s = 90°$)	about right	7×10^{15} g
Warm, dry (WD)	warmer than observed (by ~8 K at $L_s = 90°$)	about right	1×10^{15} g
Cool, wet (CW)	cooler than observed (by ~15 K at $L_s = 90°$)	~7 K warmer	2.7×10^{15} g
Cool, dry (CD)	cooler than observed (by ~15 K at $L_s = 90°$)	~7 K warmer	0.5×10^{15} g

Quality of fits to observed northern summer tropical air temperatures and northern polar ice cap temperatures are indicated in columns 2 and 3. Column 4 indicates the globally integrated vapor content of the atmosphere at the start of the simulation.

in Table 1, while the modeled annual cycles of midlevel air temperatures and northern polar cap temperatures are compared to observations in Figure 2. All simulations were at a resolution of 5° latitude by 6° longitude with 20 vertical levels, and all employed radiatively and dynamically interactive dust. The "Viking Simulation" (VS) was designed to provide the best fit to spacecraft data sets (originally from Viking, but now also from MGS) including global air temperature and surface pressure measurements. Note that the simulation does not include any dust storms or their thermal effects. The "Equilibration Simulation" (ES) differs from VS in having somewhat warmer cap temperatures, cooler air temperatures, and somewhat higher surface pressure, with the intent of speeding up the equilibration processes. Only the first component appears to make a significant difference to the equilibration processes, the latter two remaining in the simulation through heritage (i.e., the simulations were not tuned back to Viking pressures and air temperatures due to the computational burden). The four warm/cool and dry/wet simulations (WW, WD, CW, CD) were designed to allow equilibration to be approach from both sides of the stable globally averaged humidity. The warmer and cooler than observed air temperatures were set to show that equilibration to a "reasonable" vapor abundance is not excessively dependent on the bulk temperature of the atmosphere.

[26] VS does a pretty good job of fitting the annual cycle of midlevel, midlatitude air temperatures away from dust storms. Peak northern cap temperatures are reasonable, perhaps 2 K cooler than the mean of observed values. The model does capture the general shape of the observed cap temperature cycle, including the increase in temperatures above the CO_2 frost point after roughly $L_s = 50°$. This corresponds to the onset of frost removal from within the 80°–90°N circle. CO_2 frost is not completely removed from the northern polar cap until nearer $L_s = 90°$. The early, partial clearing of CO_2 from the northern polar cap is also captured in ES but in this case, the early northern summer cap temperatures are ~7 K higher than the mean of the observed values. The air temperatures in this simulation are about 5 K colder than observed during the highly repeatable northern spring and summer season. The warm cases ("warm wet" and "warm dry", WW and WD) exhibit peak cap temperatures very similar to those in the VS simulation. However, the WW and WD simulations do not show an increase in temperatures until about $L_s = 85°$. This difference in residual cap exposure between the warm and cool runs on the one hand and VS and ES on the other, results from the fact that the warm and cool series do not include

spatial variations in thermal inertia (and hence conductivity) in the polar regions (the *Vasavada* [2000] maps were only added for the VS and ES cases). Water ice has high conductivity and thus more effectively stores heat than bare ground at the same albedo (the warm and cool cases included the albedo effects of the ice caps). As a result, the VS and ES condense less CO_2 on the northern cap and become ice free earlier in the season. The WW and WD cases generate a midlevel, midlatitude cycle of air temperatures warmer than observed, by ~8 K at $L_s = 90°$. The cool cases ("cool wet" and "cool dry", CW and CD) are significantly cooler than observed, by ~15 K at $L_s = 90°$. They exhibit the same temporal evolution of cap temperatures as the WW and WD cases but have peak cap temperatures ~10 K warmer than those observed. The generation of simulations with somewhat different climates in part demonstrates the robustness of the water cycle equilibration processes operating in all of the cases.

3.1. Viking "Best Fit" Case

[27] The VS simulation provides a good emulation of the observed annual cycles of air temperature and surface pressure, without dust storms. A constant dust injection rate was used, which allowed a rough fit of the model to the annual cycle of nondust storm air temperature at midlevels (~25 km, see Figure 2) [*Clancy et al.*, 2000; *Wilson and Richardson*, 2000]. Thus interannual variability of the water cycle associated with dust storm occurrence is not addressed in this study. The annual cycle of surface pressure was tuned to the Viking Lander surface pressure observations [*Hess et al.*, 1979] by adjusting the total atmospheric mass at a given season to fit the observations. A reasonable annual cycle then results naturally from the model's CO_2 cycle.

[28] Figure 3 shows the variation of globally integrated vapor mass, surface ice, and atmospheric (cloud) ice as a function of time for 10 Mars years of the simulation. For this simulation the model was started just after $L_s = 70°$ with surface water ice north of 80°N. The atmosphere was completely desiccated, and no other surface ice deposits existed. Thus the subsequent evolution of the water cycle resulted entirely from the sublimation of water from the northern cap, its transport, and its transient condensation both in the atmosphere and on the surface.

[29] The global-integrated vapor amount shows two peaks in each model year. The first peak occurs at roughly $L_s = 130°–140°$ and is associated with sublimation from the northern residual and seasonal ice caps. The second peak is at roughly $L_s = 265°–275°$. No residual water ice cap exists in the southern hemisphere, so this release must be due to sublimation of seasonal water ice. The value of total water
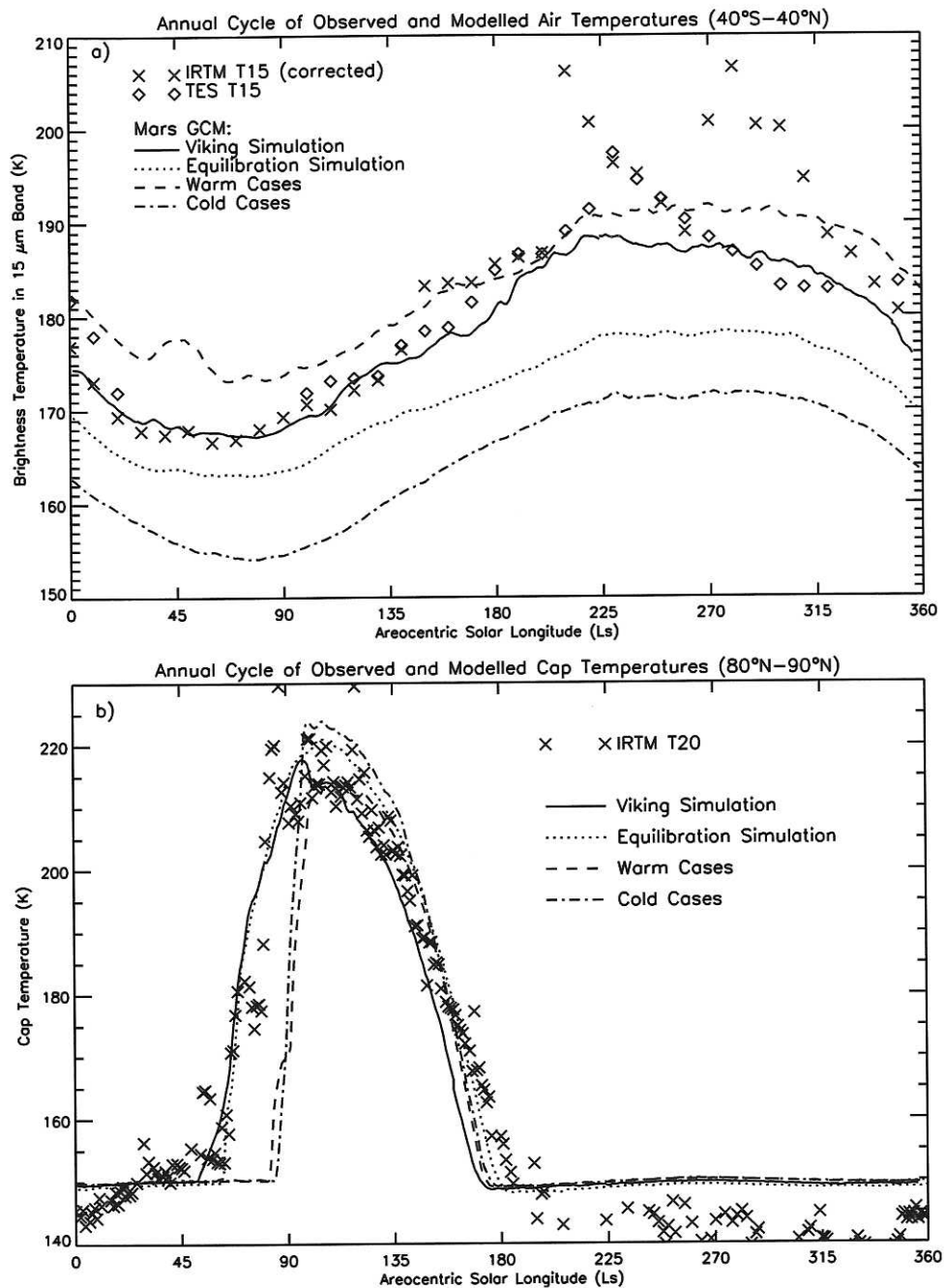
Figure 2. Summary of fits to surface and air temperature observations for simulations employed in this study. (a) Comparison with midlevel, tropical air temperatures. The model output and data from the Mars Global Surveyor Thermal Emission Spectrometer (TES) are shown. For consistency, the non-Viking data have been converted to equivalent IRTM 15-μm brightness temperatures by application of the IRTM 15-μm channel spectral response function (in the case of the TES observations) or weighting function (in the case of model output). The Viking IRTM observations have been "corrected" following the recommendations of *Wilson and Richardson* [2000]. The IRTM 15-μm channel weighting function peaks near 0.5 mbar (or 25 km), with contributions between 10 and 35 km, providing a useful sampling of the midlevel atmosphere. The data and model output have been zonally averaged and averaged over the latitude range 40°S–40°N. (b) Comparison of modeled northern cap surface temperatures and observations. The observations are provided by the IRTM 20-μm channel brightness temperatures. Both data and model output have been averaged within 10° of the northern pole. The physical lower limit on temperature is provided by the CO_2 condensation point temperature, which is near 148 K. The lower temperatures observed in winter likely correspond to scattering effects of small atmospheric or surface CO_2 ice particles [e.g., *James et al.*, 1992].
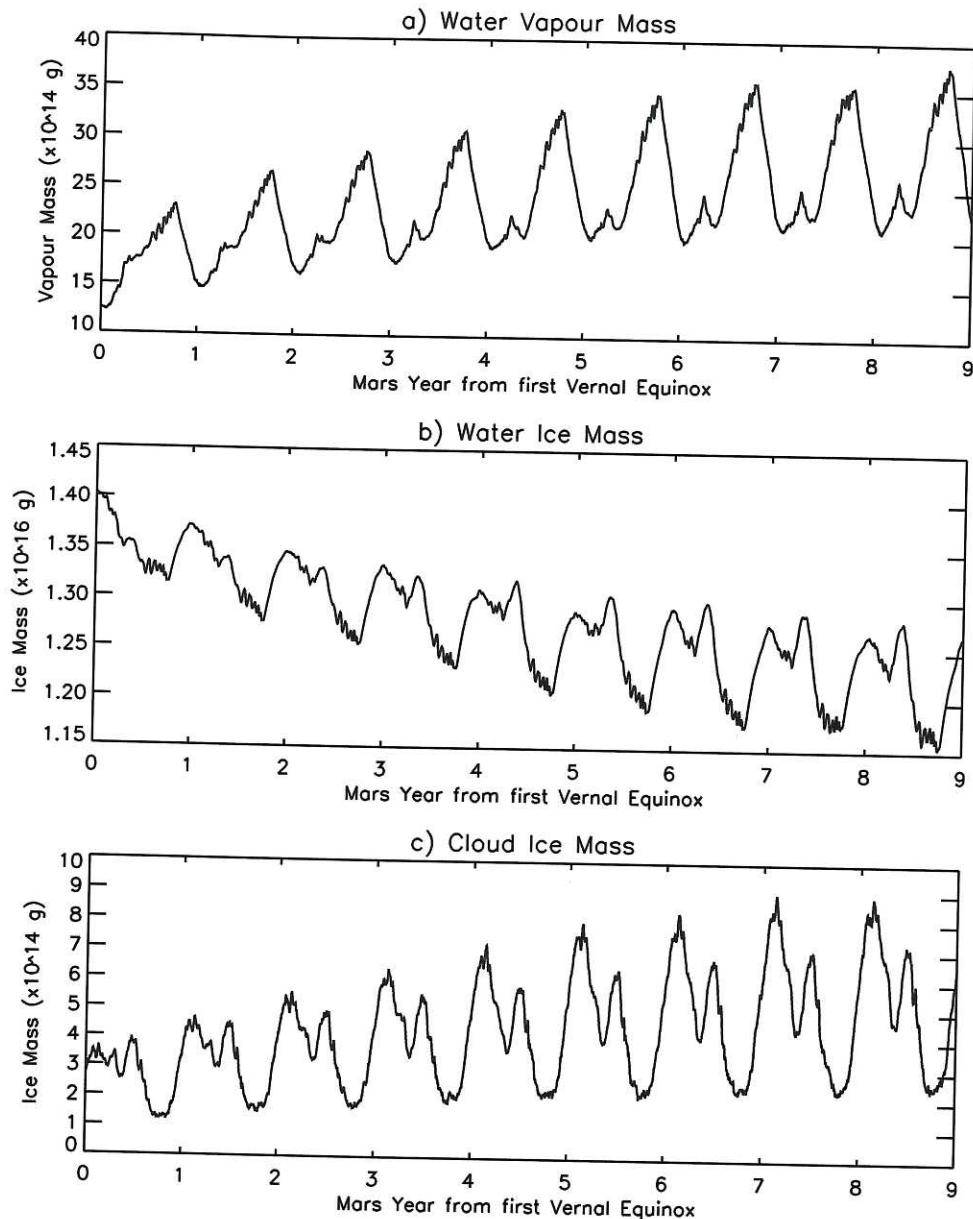
Figure 3. Water reservoir evolution for the Viking Simulation (VS, see text for details). Nine years of output are shown, starting from the first vernal equinox ($L_s = 0°$). The simulation began desiccated part way through the previous year. Budgets shown are globally integrated: (a) total atmospheric water vapor (units of 10^{14} g), (b) total surface water ice (units of 10^{16} g), and (c) total atmospheric (or cloud) ice (units of 10^{14} g). Note that absolute mass of the surface ice reservoir is meaningless and reflects only the chosen initialization value, the change in surface ice mass is significant.

vapor is high compared to MAWD observations ($2–4 \times 10^{15}$ g modeled versus $1–2 \times 10^{15}$ g observed). This overly wet characteristic is a persistent feature of the water cycle models described in this paper and is discussed more fully, below. The general trend in water ice reflects the slowing supply of water to the atmosphere from the northern residual ice cap. The larger-amplitude, annual modulations correspond to the waxing and waning of the southern seasonal ice cap, as illustrated by the strong anticorrelation with southern summer water vapor amounts and the occurrence of the modulation minima in southern summer. The secondary annual modulation on both the water vapor and water ice budgets reflects formation and sublimation of the northern seasonal ice cap. The annual double maxima in water ice cloud amount correspond to cloud formation in the polar hoods in both spring and autumn, with the first spike in each year being larger and longer sustained due to the additional cloud generated in the tropics during late spring and summer [see *Richardson et al.*, 2002].

[30] It is interesting to note that the primary peak in modeled, globally integrated water vapor occurs during southern summer. Figure 4 provides some insight into how this situation arises. Figure 4 shows the latitudinal distribution of vapor and surface water ice as a function of
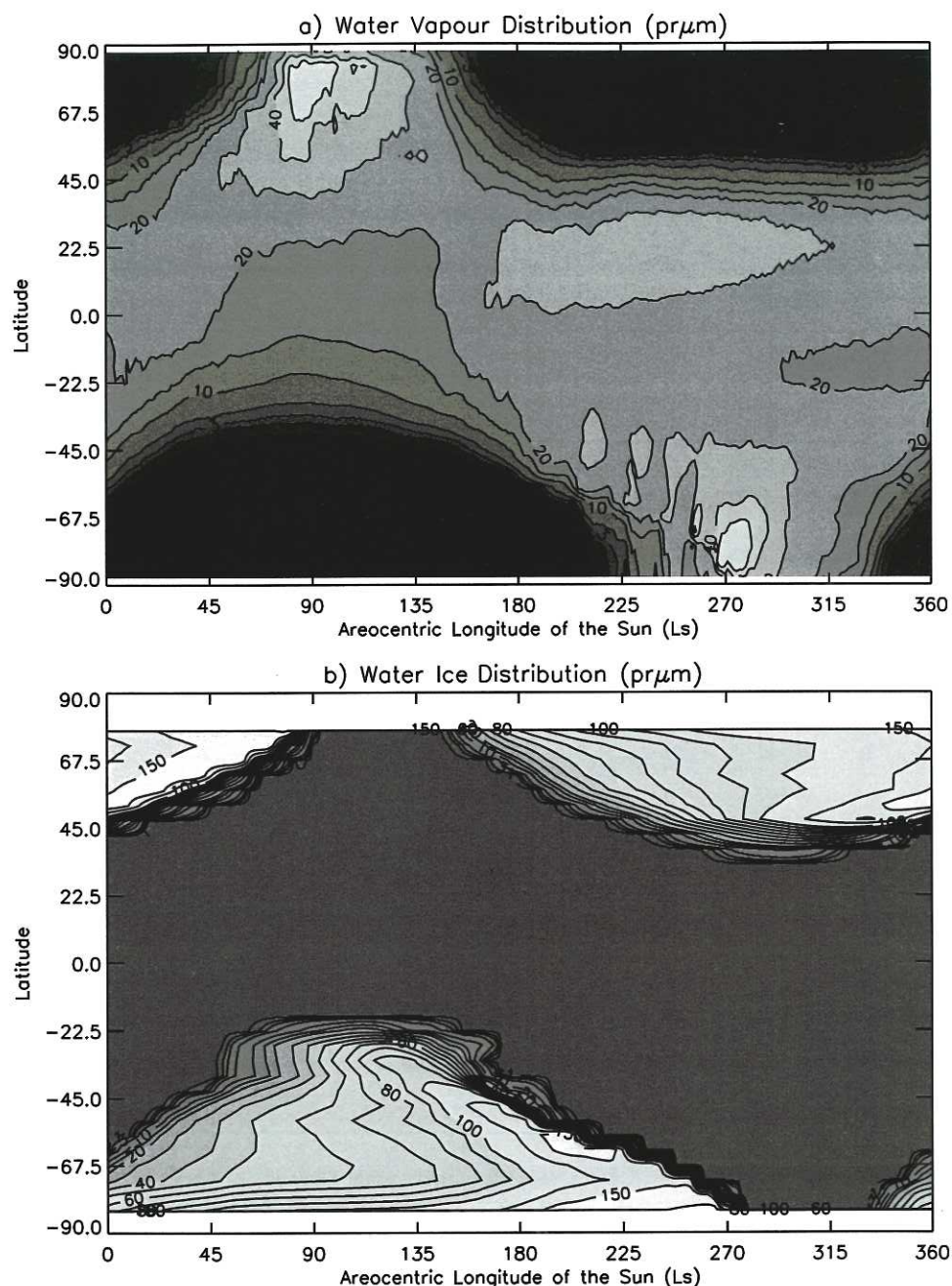
Figure 4. The latitudinal and seasonal distribution of water vapor and surface water ice in the ninth year of the VS simulation. (a) Water vapor in units of prμm for comparison with the data in Figure 1. Contouring and shading levels are at 1, 2, 3, 5, 10, 20, 30, 40, and 50 prμm. (b) Surface water ice. Shading and contouring at 1, 2, 3, 5, 10, 20, 30, 40, 50, 60, 70, 80, 100, 120, and 150 prμm. Note that the maximum mass of the seasonal cap at any latitude occurs just before the seasonal cap is sublimed in spring.

season for the ninth year of the simulation. The primary peak in southern summer water vapor occurs poleward of 40°S, with a maximum value above 50 prμm near 80°S. The vapor accumulates rapidly at high latitudes in the period L_s = 250°–270°, which is the final phase of the seasonal CO_2 ice cap retreat, but increases throughout southern spring in the vicinity of the cap edge. It can be seen in Figure 4b that at a given latitude within the seasonal ice cap the maximum ice content of the cap occurs just before its sublimation.

Thus accumulation of water ice at the cap edge is ongoing even when the ice is being warmed by increasingly intense sunlight after polar dawn. What is going on here is that as the leading edge of the seasonal ice cap is sublimed, the water that is released into the atmosphere has some chance of being mixed (by any number of mechanisms) poleward over the nearby seasonal ice cap. Once over the new edge of the seasonal ice cap, there is a strong likelihood of recondensation. This process is continually repeated, allowing

water ice to "creep" poleward, and thus there is a tendency for the rim of the seasonal ice cap to transport water poleward via this quasi-solid-state creep mechanism. This cannot continue indefinitely, as ultimately the seasonal ice cap will reach the pole and expire. The mechanism operates at both poles and was also seen by H97. In the north this transport serves to return some of the water lost from the residual cap the previous summer. In the south the mechanism provides all the vapor observed to accrue in the high southern polar latitudes. It also provides a mechanism for permanently trapping water on the southern residual CO_2 ice cap. The strength of this trapping mechanism depends on how effectively vapor is vertically mixed out of the clutches of the polar cold trap. If the cold trap maintains good contact with the sublimed seasonal water vapor (as might be expected in a one layer atmosphere, such as that of *Jakosky* [1983b]), it can be very effective at permanently removing water. This might explain the ability of the *Jakosky* [1983b] model to produce relatively low southern hemisphere vapor amounts, despite using temporally uniform atmospheric diffusivity. It is equally clear that the overabundance of water vapor predicted by the model described in this paper results from too much water getting into the southern seasonal ice cap and/or too much water escaping from the southern residual ice cap.

[31] A significant amount of water was found to exchange between the hemispheres during the annual cycle. This is in stark contrast to what would be expected on the basis of the *Haberle and Jakosky* [1990] study but is consistent with the only other 3-D water cycle model study (H97). Figure 5 shows the mass of water vapor (Figure 5a) and the change in the total mass of water (Figure 5b) in each hemisphere during the simulation. The vapor plot shows the southern hemisphere to have a strong, single maximum each year, while the northern hemisphere has two maxima of smaller amplitude. The secondary peak in vapor in the northern hemisphere occurs during northern winter. It can be seen in Figure 4 as the vapor maxima around 20°N. The maintenance of high vapor amounts in the northern tropics during northern winter, but the absence of large vapor amounts in the southern tropics during southern winter, gives rise both to the maximum in globally integrated atmospheric water vapor in southern summer and the rather different behavior of the northern and southern hemispheric-integrated vapor amounts. It is a fundamental asymmetry in the modeled water cycle. Although the global vapor mass histories derived from MAWD data do not show a southern summer vapor peak (some caution in using MAWD data as a gauge of southern spring and summer vapor should be exercised due to the obvious impact of dust storms on these data), the latitudinal MAWD data (Figure 1) do show strong evidence for a northern tropical vapor maxima during the relatively clear interval between the 1977a and 1977b storms (again, this aspect of the MAWD data appears to be confirmed by TES vapor observations [*Smith*, 2002]). This maxima has not been produced in any previous model of the water cycle but results naturally in this model from the combined effects of Hadley cell transport and the difference in mean elevation of the northern and southern tropics [*Richardson*, 1999].

[32] In general, the model produces a reasonable, qualitative fit to the observed vapor distribution. A peak in vapor is reproduced in the northern polar regions in northern summer, with vapor amounts decreasing monotonically to the southern pole. A secondary maxima in vapor is observed in the southern polar regions in southern summer during the brief, relatively clear period in the Viking observations, and is also reproduced. Encouragingly, the model also reproduces the northern winter tropical vapor maxima, unlike all previous water cycle models. Differences between the model and observations do not relate to the shape of the latitude-time vapor distribution so much as the actual vapor amounts (the primary exception being the "slope" of the peak water vapor tongue toward earlier seasonal dates, rather than later seasonal dates as observed). The southern polar summer maximum is overrepresented, and the model is too wet in general. This reflects an over effective transport of water from the northern polar cap or underefficient trapping of water on the southern residual ice cap. In either case, the model provides a useful test bed for examining the water cycle systemic behavior, with the knowledge that some of the elements of the machine are running at incorrect "rates."

[33] The degree of water movement between the hemispheres is an interesting quantity to assess as it provides a gauge of global mixing of water between reservoirs (i.e., it allows one to assess the degree to which the water cycle is a series of local, vertical exchange processes or a globally coupled, horizontal process). Figure 5b provides a direct measure of the amount of total water exchange between the two hemispheres. In this simulation, roughly 1.5×10^{15} g of water is seen to be "sloshing" backward and forward between the hemispheres each year. This is roughly equivalent to the peak mass of vapor observed in the atmosphere [*Jakosky and Haberle*, 1992], and a little less than half the peak vapor amount predicted in this model. Thus a significant amount of water exchanges between the hemispheres, and hence the modeled cycle cannot be considered primarily a local exchange of water.

[34] The role of clouds in the water cycle is discussed in detail by *Richardson* [1999] and *Richardson et al.*, [2002]. However, some gauge of the behavior of clouds can be gleaned from Figure 5c. Here, water ice trends for northern (>30°N), southern (<30°S), and tropical regions (30°S–30°N) are shown for the 10 simulated years. The northern and southern ice cloud trends possess double maxima each year. These peaks occur in both hemispheres when the seasonal CO_2 ice is subliming and water is being released into a cool atmosphere, and in the late summer, when air temperatures fall and the seasonal ice cap is reforming. Much larger peaks occur in the tropics but only during northern summer. These peaks corresponds to the tropical cloud belt observed by Viking [*Tamppari et al.*, 2000] and MGS [*Pearl et al.*, 2001] but first recognized as an important feature of Martian meteorology in Hubble Space Telescope observations by *Clancy et al.* [1996]. The peak cloud ice amounts predicted in this model are roughly 25% of the peak vapor amounts and are thus likely unrealistically high (this is hard to properly gauge due to the porcity of cloud ice mass measurements). *Richardson et al.*, [2002] evaluate this feature of the modeled cycle in greater detail.

[35] It is clear from Figure 5b that the water cycle produced by this simulation has not yet come into a steady state by the end of 9 Mars years by virtue of the fact that the
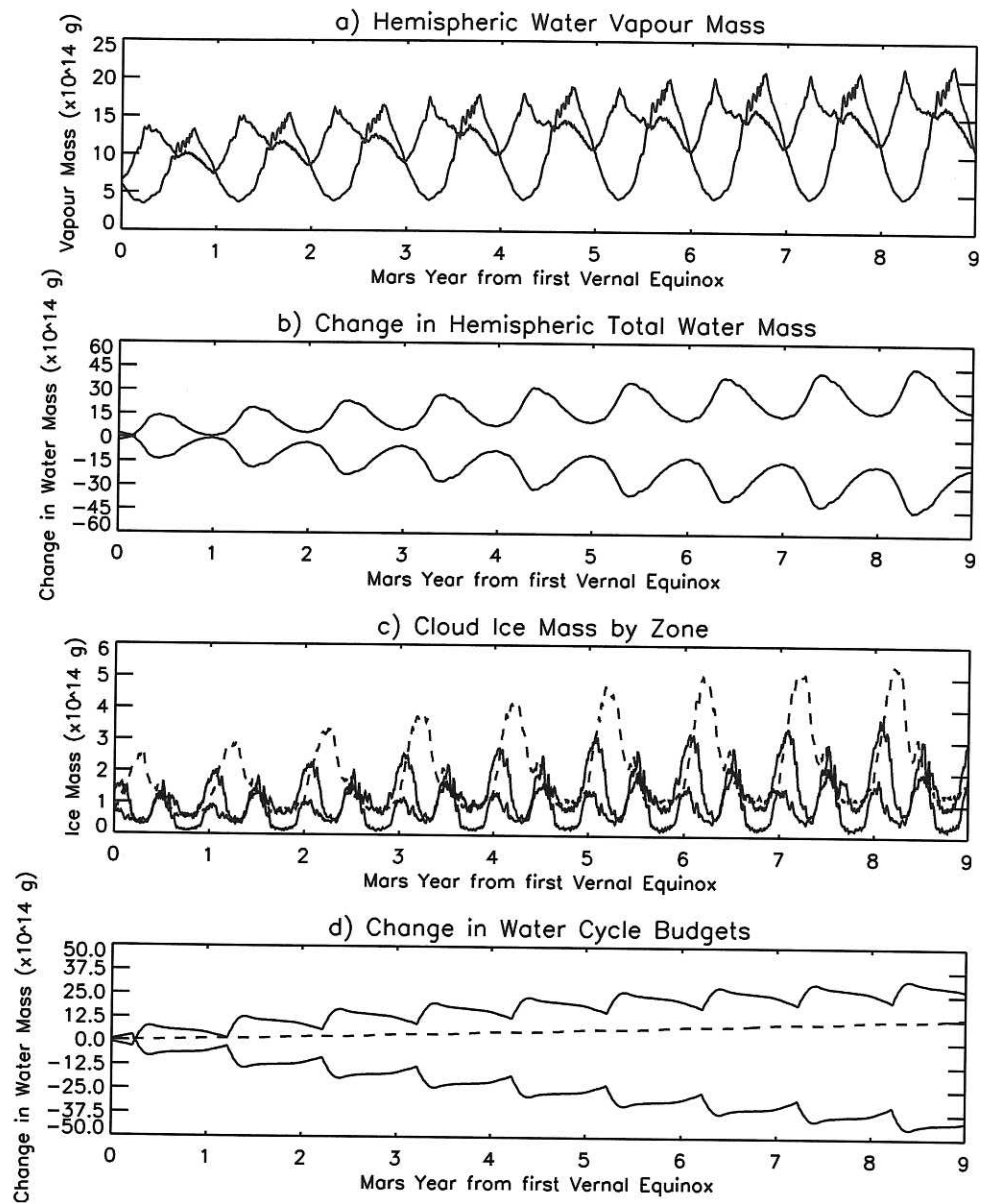
Figure 5. The evolution of water budgetary elements for the VS simulation over 9 model Martian years. (a) The mass of water vapor in each hemisphere. Solid line is southern hemisphere vapor while the dash, triple dot line is northern hemisphere vapor. (b) Total water (ice and vapor) in each hemisphere. Solid is southern hemisphere, dash, triple dot is northern hemisphere. (c) Atmospheric water ice (cloud, haze, etc.) in each of three bands. Solid represents atmospheric ice south of 30°S, dash represents tropical atmospheric ice (between 30°S and 30°N), dash, triple dot represents atmospheric ice north of 30°N. (d) Water ice budgets defined in Figure 6 and in the text. Dotted line is the change in all water (vapor and ice) north of 75°N, dashed line is the change in surface water ice south of 85°S, and the solid line is the change in all other system water.

southern hemisphere is still seen to be gaining water from the north. Further, it is not clear that the hemispheric trends are actually close to stabilization (Figure 5b). It is also difficult to assess what is happening mechanistically within the water cycle with any of the plots shown to this point. For this reason, we have chosen to develop a new system of water budgets that provide greater insight and will be used extensively in the following sections (and in the work by *Richardson et al.*, [2002], discussing the effects of water ice

clouds). The components of the water cycle in this system are graphically illustrated in Figure 6. As the northern residual ice cap provides the only source for water at model initialization, we chose to monitor this reservoir. We actually monitor the whole column over the northern cap (75°N–90°N) including the surface ice, water vapor, and ice in the atmosphere. If water simply moves vertically between the surface and atmosphere, for example, in response to heating and cooling of the cap in summer and winter,
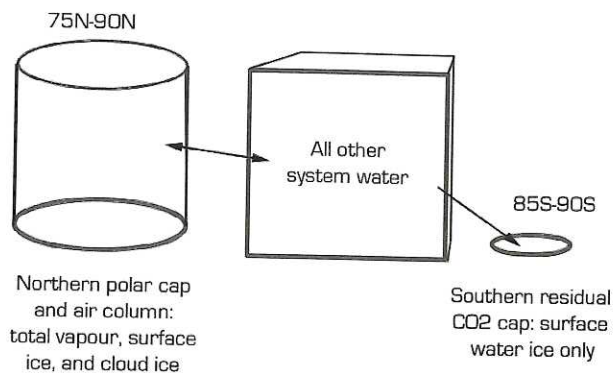
Figure 6. A cartoon definition of the water budgetary elements defined to assist in assessing the method of evolution and equilibration of the model water cycle. Three budgetary elements are considered: Northern polar water, which includes all water substance north of 75°N, surface water ice trapped on the southern residual CO_2 ice cap, and all other system water (the combined mass of all water not included in the other two elements). The one-way arrow indicating exchange between the "other water" and "southern cap" elements indicates that once water is cold trapped upon the CO_2 ice cap, it cannot escape.

respectively, we do not recognize it has having sensibly left the residual cap system (it has not contributed to the global water cycle). Another reservoir is provided by the southern residual ice cap (85°S–90°S). As this ice cap is permanently composed of CO_2, by model prescription, it is a permanent sink for water, which needs to be monitored. In this case, we do not include the southern polar atmosphere, as any water not actually bonded to the southern residual cap retains the potential for transport away from that cap (it has not yet been caught in the cold trap). For simplicity, we treat all other water as a third budgetary element. This includes vapor, cloud ice, and seasonal surface ice not contained within the two polar reservoirs. The nonpolar water inventory will change as a consequence of gain or loss of water from the northern polar column, and loss to the southern polar cap.

[36] The water budget plots for the VS simulation are shown in Figure 5d. In this case, the northern polar column budget is shown as the decreasing dotted line, while the nonpolar water is shown as the increasing solid line. As the simulation was begun with water only present on the northern polar cap, these trends clearly show the global moistening process. This plot shows that the model is not yet nearing steady state, although the rate of water loss from the northern polar column is lessening. We will discuss the details of the annual spiking in the northern polar and nonpolar water budgets in a later section. These provide direct insight into the mechanisms of equilibration. "Equilibration" is, in fact, a misleading term. As can be seen from the southern polar budget, there is continuing, steady, irreversible loss of water to the southern cap at a rate of $\sim 1.4 \times 10^{14}$ g/Mars year, in reasonable agreement with the observed estimates of *Jakosky* [1983b]. Thus the best that can be attained is a steady state in which the nonpolar water budget is repeatable from year to year,

with net loss from the northern polar column balancing net gain at the south pole.

3.2. Bounding Equilibrium: Water Cycle Stability With High and Low Initial Vapor

[37] The simulation discussed in section 3.1 was not run out to the attainment of a steady state. The primary reason for this was the computational cost in running simulations for multiple years (after 9 Mars years the simulation was still far from steady state and so it was cut off). However, as a consequence, the question of whether this model atmosphere would continue to accrue water vapor and flood has not really been addressed. The simulations presented in this section were undertaken before those described in the last section and are described by *Richardson* [1999]. The goal of these experiments was to determine whether equilibration would occur at reasonable globally integrated vapor amounts without having to drive the model all the way to steady state. This was undertaken by initializing different model simulations with global water loads significantly lower and significantly higher than observed. For example, the "cool" runs, CD and CW, were initialized with loads of 0.5×10^{15} g and 2.7×10^{15} g of water, respectively (see Table 1) as compared to average observed vapor loads of $1-2 \times 10^{15}$ g. Given that these values of initialized water bracket the observed amounts, the modeled budgets should produce opposite trends, driving toward some middle state, if the modeled water cycle is close to representing the real cycle. In addition, at the time these simulations were undertaken, there was still considerable uncertainty in the mean state and degree of interannual variability of midlevel atmospheric temperatures [*Richardson*, 1998]. Thus simulations were undertaken for rather extreme atmospheric temperatures (as controlled by atmospheric dust, which also significantly impacts the global mixing efficiency of the atmosphere via the large-scale circulation). These simulations now serve as valuable indicators of the sensitivity of the water cycle to changes in annual average forcing.

[38] Figure 7 shows the budget curves (as defined in Figure 6) for the simulations WD, WW, CD, and CW, where the first two and last two constitute simulation pairs. In all four cases, the southern residual ice cap accrues water, as in the VS simulation. It should also be noted that the annual shapes of the other two budgetary elements closely resemble those produced by VS. Examining the "warm" simulations first, it is clear that the dry and wet cases show opposite budgetary trends. The dry case (WD, Figure 7a), as with VS, shows ongoing loss of water from the northern polar column, while the nonpolar water increases. In contrast, the wet case (WW, Figure 7b) now shows the northern polar column gaining water at the expense of the nonpolar water budget. Comparing the behavior of the northern polar column water, the distinction between gain and loss is physically manifested as a change in the relative volume of water inflow during northern autumn, winter, and spring, and water outflow in summer.

[39] The "cool" simulations show very similar behavior to that of the warm series. In the dry case (CD, Figure 7c) the northern polar column supplies water to the rest of the system, while in the wet case (CW, Figure 7d) the northern polar column soaks up excess water from the nonpolar
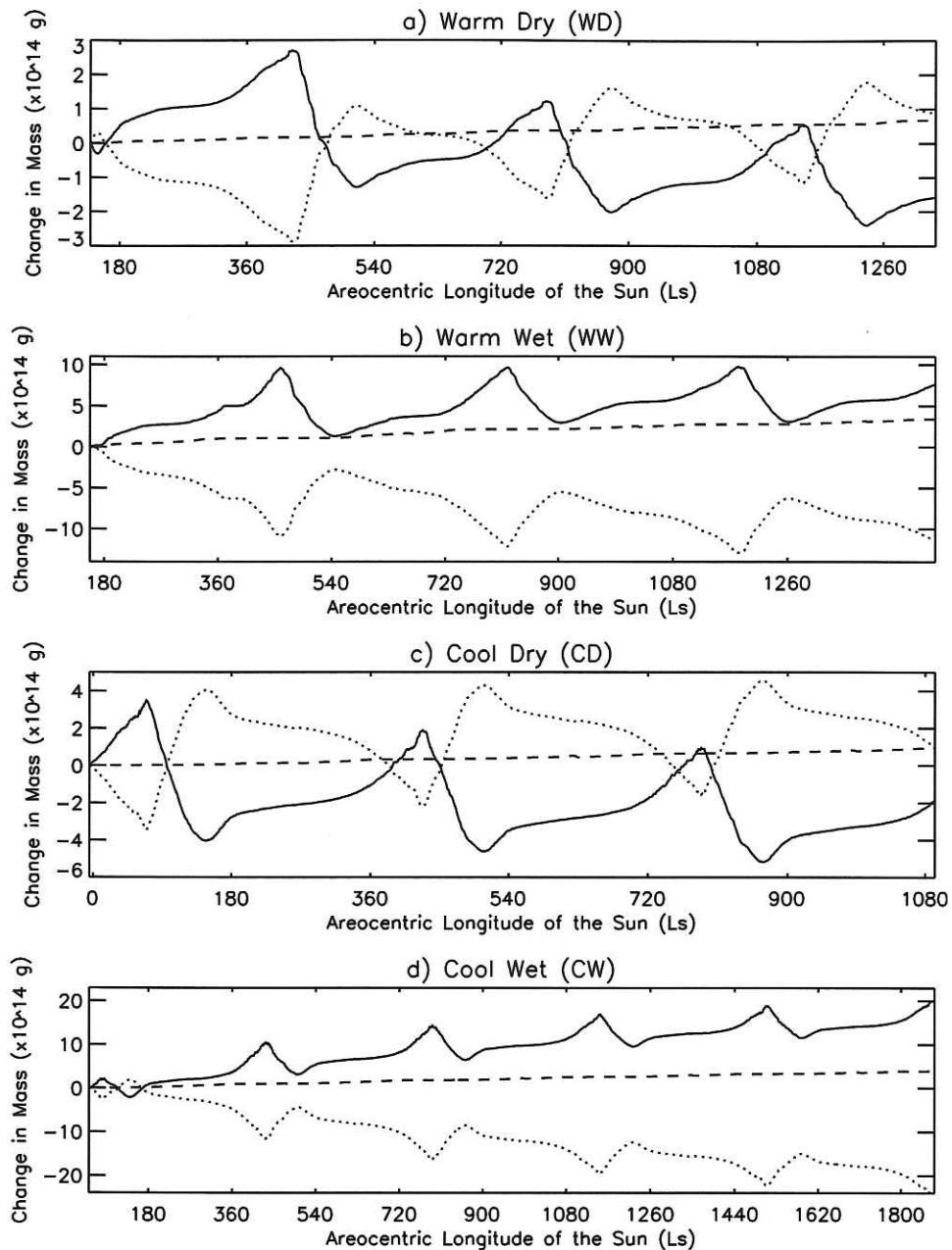
Figure 7. System water elements for four simulations. The simulations were undertaken to demonstrate that when initialized with vapor amounts higher and lower than the "equilibrium" value, the water cycle exchange mechanisms drive the system back toward the equilibrium state. Budgets are as defined in Figure 6. In each case, the solid line is northern polar water, dashed line in south polar water ice, and dotted line is all other water. Panels represent two pairs of runs (the warm series, WD and WW, and the cool series, CD and CW) differing within each pair only in initialized water amounts (see Table 1 for simulation definitions). The two pairs differ from each other in terms of background air temperature and circulation vigor (see Figure 2 and Table 1).

water reservoir. The distinction between the two cases in the cool series is again the relative volume of nonsummer flow to the northern pole versus summer flow from it. The distinction is primarily manifested by changes in the nonsummer return flow volume. While the outflow changes little between the two cases, the inflow varies from 5×10^{14} g to 1×10^{15} g, changing a net outflow to a net inflow.

[40] The primary conclusion derived from the warm and cool series is that the model shows a tendency toward an equilibrated state (or more correctly, steady state) that is not far (within a factor of a few) of the observed vapor amount. This contrasts sharply with the finding of H97 that the model would flood without regolith adsorbate acting as a buffer, and that of *Haberle and Jakosky* [1990] that an adsorbate source is necessary to keep the atmosphere from
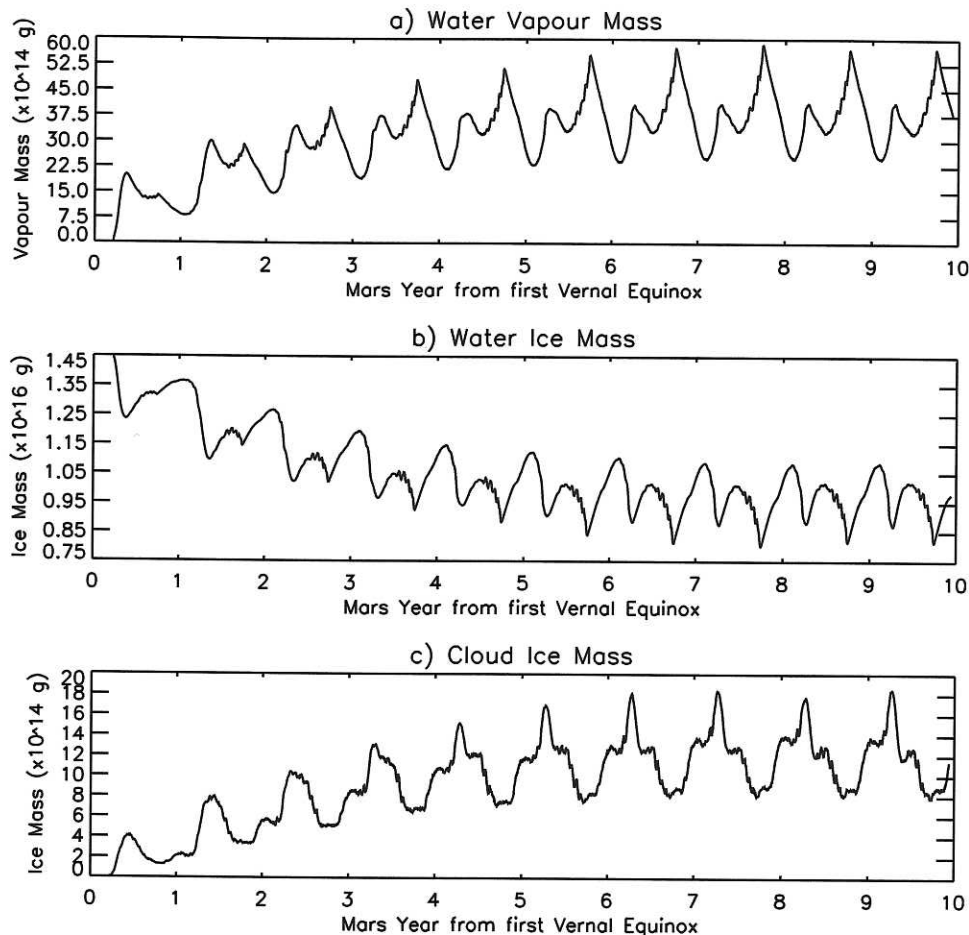
Figure 8. Same as Figure 3 but for 10 Mars years of the equilibrium simulation (ES).

becoming desiccated. Thus a regolith does not appear to be essential for producing a reasonable emulation of the observed cycle.

3.3. Attainment of Equilibration

[41] The cool and warm series simulations described in section 3.2 suggest that the model should generate an equilibrium or steady state that is not very different from that observed. However, none of these runs, or the VS case actually ran to equilibrium. In order to demonstrate that the model will, in fact, "equilibrate" we conducted an additional simulation, with air temperatures near to those observed (if a little cooler, see Figure 2) and with slightly higher peak cap temperatures. The effect of these differences from the VS case is to make the equilibrium simulation (ES) somewhat more wet. This serves to speed-up the simulation and hence the attainment of equilibrium. Figure 8 shows the globally integrated amounts of vapor, surface ice, and cloud ice in this simulation. When equilibrium (steady state) is reached, the global vapor mass varies between $3-6 \times 10^{15}$ g (versus $2-4 \times 10^{15}$ g for VS and $1-2 \times 10^{15}$ g observed). The simulation was begun dry, and thus the increase in atmospheric vapor (and cloud ice) comes from the sublimation of surface ice. The latitude-season distribution of zonal-average vapor is shown in Figure 9. The behavior is very similar to that of the VS case (Figure 4) except that the vapor amounts are now higher

(by ~50%). The budgets for the ES case are shown in more detail in Figure 10. These can be compared with the budgets for the VS case in Figure 5. It can be seen from Figure 10b that net interhemispheric transport terminates after year 6 or 7. This length of simulation also sees the end of water ice cloud build up and the flattening of the annual trends in the northern polar column and nonpolar water budgets in Figure 10d.

[42] The most important result shown in Figures 8 and 10 is that the water cycle does equilibrate: the cycle does settle into a repeatable annual pattern. Although the vapor amounts are high (~3 times those observed) the model is in no sense "flooded" as described in the regolith-free simulations of H97. It is certainly not dry, either [cf. *Haberle and Jakosky*, 1990]. In the ES case this high vapor amount is most directly related to the excessively thick atmosphere. Thus, as suggested by the cool and warm series simulations, the modeled water cycle will equilibrate (or more accurately, come to a steady state) without a regolith. Further, the water cycle equilibrates rather quickly, within the first 6 Mars years. This equilibration timescale is rapid compared with the nonregolith simulation described in H97 but is consistent with more recent results from their model (H. Houben, personal communication, 1999). In fact, we have seen that the VS simulation will not equilibrate quite so quickly, but likely within a factor of 2 or so of this number. Thus the

Water Vapour Distribution (prμm)
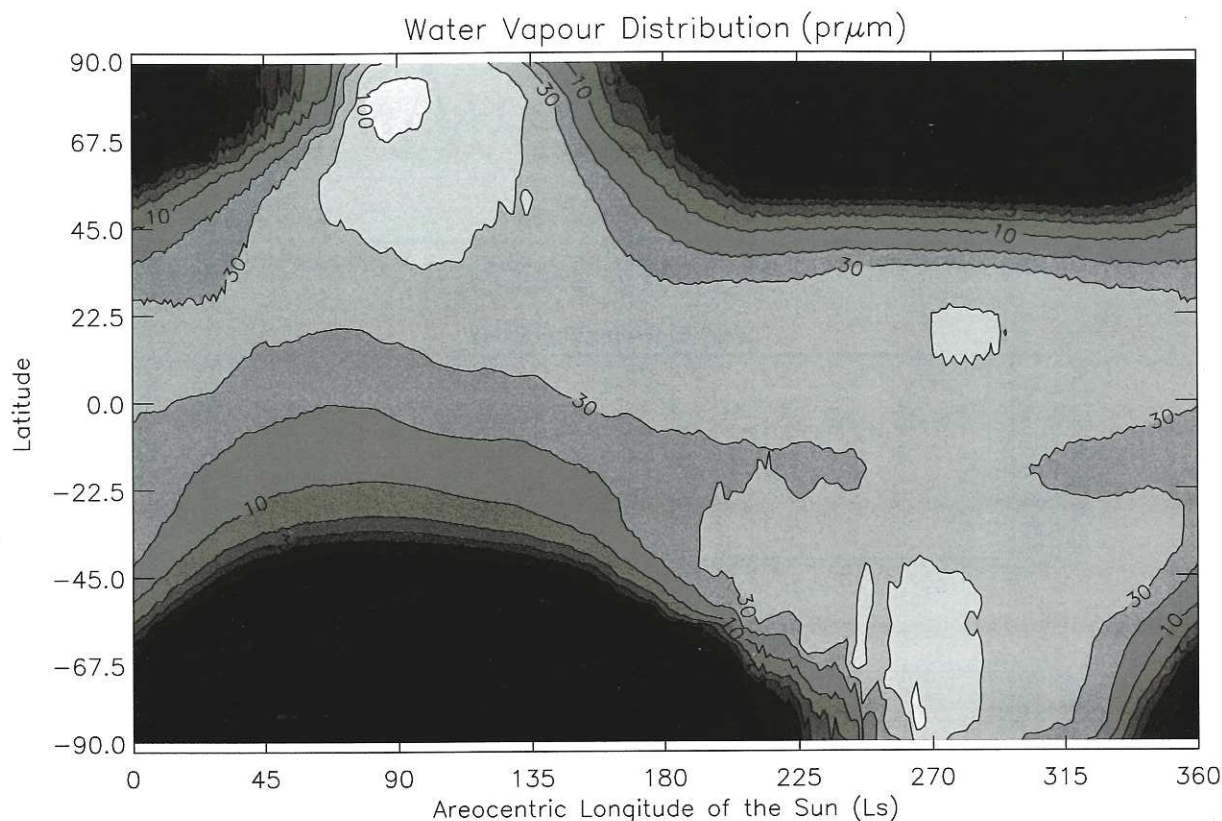
Figure 9. Same as Figure 4a but for the ninth year of the ES case.

tendency for the water cycle to return to a quasi-equilibrium state is quite strong; i.e., the e-damping time on perturbations is of order 10 Martian years (in these simulations).

3.4. Mechanism of Water Cycle Equilibration

[43] The global water budget elements defined in Figure 6 provide a formulation for the water cycle that allows some insight into the mechanisms of the equilibration process. As discussed in section 3.1, the three budget components correspond to the total water north of 75°N (vapor plus surface and atmospheric ice), the mass of water ice south of 85°S, and the sum of all other water in the modeled system. The surface water ice at the south pole is effectively cold trapped by the perennial presence of CO_2 ice at those latitudes and therefore "lost" from the water cycle. Thus the water cycle never achieves a true equilibrium, as there is a near continuous loss of water to the south. In nonregolith simulations the north polar cap provides the only long-term source and sink for global water, while the water that exists in the rest of the climate system will increase or decrease depending on the fluxes of water into the south polar cap, and into and out of the north polar region.

[44] Examining Figures 5d, 7, and 10d, it can be seen that during late northern spring and summer, the north polar region loses water to the rest of the system. This loss from the northern polar column begins in midnorthern spring (around $L_s = 45°$) in the VS and ES cases, and later (nearer $L_s = 70°$) in the cool and warm series simulations. These differences are directly related to differences in the onset of

cap temperature increases (see Figure 2). The fact that the northern polar region is losing water before the residual cap is exposed demonstrates that early in the season, this water is being provided by sublimation of seasonal water ice. By solstice the water is coming from the northern residual ice cap itself. The sharp decrease in northern polar water through late northern spring and early northern summer corresponds to a rapid transport of water equatorward. However, it can be shown that the polar circulation in northern summer, and specifically the meridional transport, is relatively weak compared to that at other seasons (though substantially stronger in the 3-D simulations than in 2-D) [*Haberle and Jakosky*, 1990; *Houben et al.*, 1997; *Richardson*, 1999]. This large flux is driven by very strong meridional gradients in vapor evident in Figure 4 (and in observations, Figure 1).

[45] By late northern summer the northern polar vapor outflow has been stemmed, and is reversed to yield a sharp, strong influx of vapor (around $L_s = 150°$). The influx at this time corresponds to relatively high northern polar vapor amounts and the onset of strong cooling in the northern polar interior. The northern polar westerlies are beginning to reestablish and instabilities on the newly developed front provide strong mixing of water back into the pole. As autumn proceeds, the polar vortex wall and accompanying eddies move equatorward and little water mixes very deeply into the region poleward of the vortex. This is represented by the flattening of the northern polar vapor inflow between $L_s = 200°$ and $L_s = 320°$.

[46] As spring arrives at the northern pole, the northern polar vortex is contracting, bringing vapor and eddies
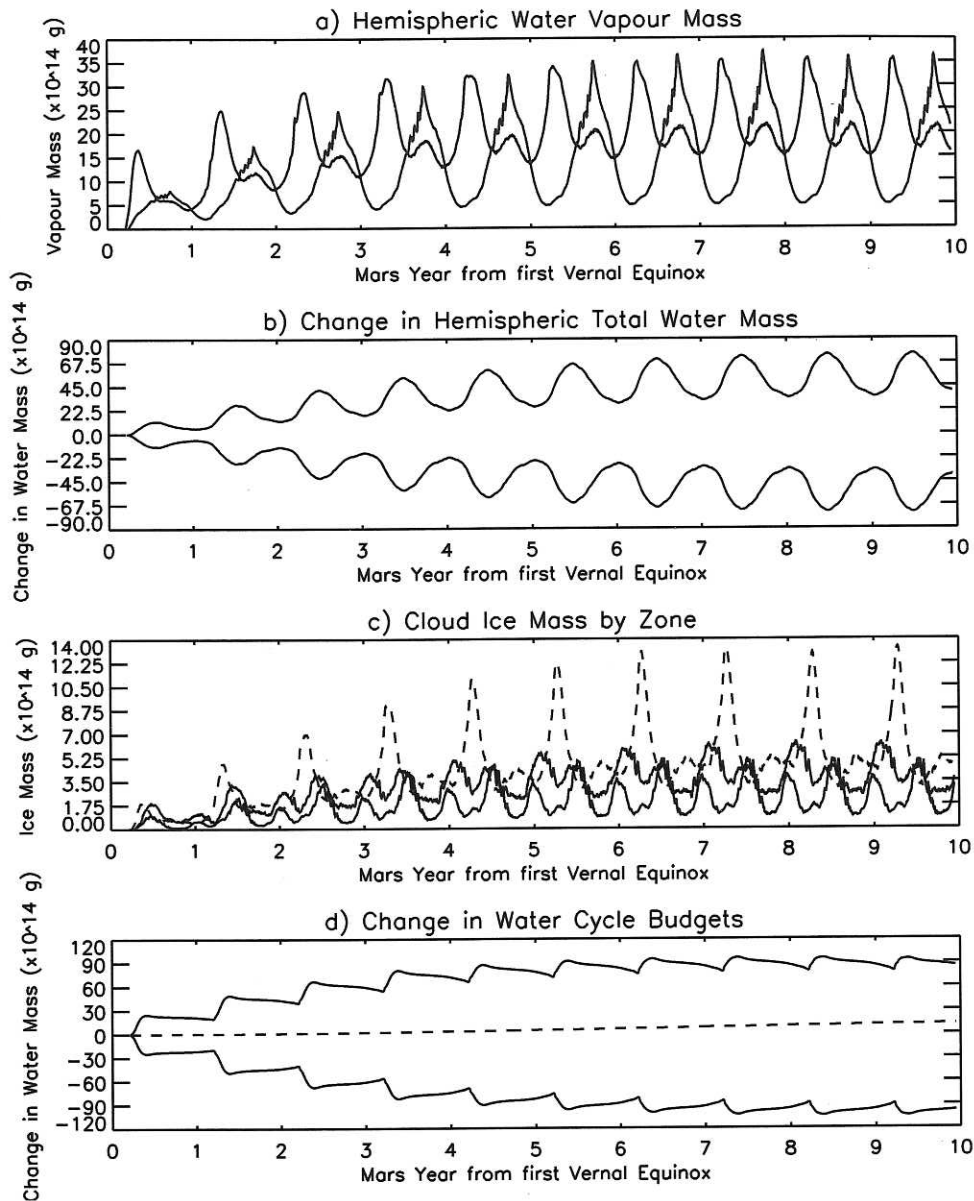
Figure 10. Same as Figure 5 but for 10 Mars years of the ES case.

within reach of our northern polar budgetary region. This partially accounts for the increased inflow of vapor. In addition, some water arrives via a quasi-solid-state mechanism described in section 3.1. This water is carried along the retreating edge of the seasonal ice cap through a process of continuing sublimation, poleward mixing, and recondensation. Finally, by mid-to-late northern spring, sufficient CO_2 ice has been removed from the northern polar budgetary region for water ice to sublime once more, regenerating the northern spring and summer vapor gradient and outflow.

[47] Figure 10d shows that as the simulation nears and achieves equilibrium, the relative magnitudes of the summer outflow and nonsummer inflow adjust until the outflow is balanced by the inflow plus the small mass of water lost to the south pole. Figures 7a and 7b show water budget components for simulations in which the model was initialized with water amounts significantly lower than and significantly higher than observed. Thus they bracket the

equilibrium amount and approach it from both sides. In these cases and that for equilibration from a dry state, the distinction between simulations experiencing accumulation and those experiencing loss of north polar water lies solely with the relative magnitudes of the winter influx and summer outflux. The factors determining these fluxes therefore determine whether the north polar cap is an annual average sink or source for global water vapor.

[48] On seasonal timescales the sole process responsible for the transfer of water between the north polar region and the rest of the planet is dynamic mixing of atmospheric vapor and cloud ice (even in the case of the quasi-solid-state ice trapping, atmospheric mixing is key). The magnitude of the transfer flux will depend on the vigor of mixing and the latitudinal vapor or ice gradient. Figures 4 and 10 show that during northern summer there is a large north polar-to-extratropical gradient in vapor and that this gradient greatly weakens in magnitude and reverses during the rest

of the annual cycle. Generally, similar patterns of vapor distribution occur for the simulations used to produce Figure 7. The nonsummer gradient depends entirely on the background tropical and extratropical vapor amount, as there is little or no vapor in the northern polar region. The amount of tropical and extratropical vapor is history dependent and reflects either the amount placed in the model at initialization, or the amount thus far extracted from the north pole. In contrast, the northern summer gradient is the difference between the vapor mass driven off the north polar cap and the tropical/extratropical background level. However, the tropical/extratropical background vapor column density is roughly 10% of the polar value, and thus the mixing ratio gradient during summer results, to first order, only from the vapor column driven off the cap. As discussed by *Richardson* [1999] and *Richardson et al.*, [2002], the north polar cap surface temperature primarily determines the polar vapor column. Thus the summer and nonsummer gradients in vapor are controlled by independent parameters: the history-dependent global vapor amount (nonsummer) and the north polar cap surface temperatures (summer).

[49] All else being equal (i.e., were the mixing capacity of the atmosphere to remain constant year-round), the northern summer requires a much larger gradient in vapor mixing ratio in order to produce an outward flux capable of balancing the return flux of vapor, for two reasons. First, the northern cap is fighting an "up hill battle" in that vapor moved equatorward is effectively "diluted" by the much larger volume of lower latitudes. For example, 1 prμm of vapor per degree longitude moved from 80°N becomes 0.27 prμm per degree longitude at 50°N. So the northern summer circulation has to work much harder to reduce the northern summer vapor gradient than does the return flow in the nonsummer periods. Second, the outflow of vapor only occurs during northern summer, roughly 1/6 of the annual cycle. The remaining 5/6 of the year are left for the return flow. Thus the very large vapor gradient in summer is required to produce a vapor flux that can compensate for the nonsummer return flow.

[50] Combining the behavior of vapor gradients and mixing capacity as a function of season, the following paradigm for the model water cycle develops. During summer the northern cap will export to the rest of the planet a fixed amount of water that to first order is only dependent on north polar cap temperatures. During the rest of the year the circulation returns to the north polar cap an amount of water that depends, again to first order, only on the amount of water sitting in the tropical/extratropical atmosphere. This separation of dependencies means that if we overinitialize the model (or the atmospheric water amount is perturbed high by some process), the action of the strong nonsummer circulation on the polar/extratropical gradient of vapor more than compensates for the "fixed" summertime export of polar water by the action of the effectively "weak" mixing on the much larger gradient in vapor. Conversely, a low or dry initialization will lead to the polar water export overwhelming the nonsummer return flow. This self-regulation mechanism is clearly evident in the behavior of the model water budgets shown in Figures 5d, 7, and 10d. By these means the model will supply polar water to the rest of the planet when underinitialized or

perturbed low, and soak up water when overinitialized or perturbed high.

[51] The southern cap acts as a permanent sink for water in all of the simulations examined. This is a trivial result of prescribing a permanent CO_2 ice cap at the south. The amount of mass lost to the southern cap is likely overestimated in these simulations if the excessive "wetness" of the simulations results from overvigorous north-south transport, or underestimates loss if the "wetness" results from underefficient southern polar trapping. In any case, the value predicted from this model is uncertain to over an order of magnitude but is centered near 10^{14} g/Mars year. This number is consistent with modeling by *Jakosky* [1983b] and with estimated "upper limits" by *Jakosky and Farmer* [1982]. This corresponds to the addition of an annual water ice layer of a few tenths of millimeters to a few millimeters thickness.

4. Importance of Condensation Flow

[52] Condensation flow is the globally integrated net pole-to-pole flow associated with the cyclical condensation and sublimation of CO_2 ice deposits at the poles. This flow is nonnegligible because such a large fraction of the bulk atmosphere participates (there is a roughly 25% mass cycling over the course of a year). The flow results directly from the spatial patterns of pressure generated by the additional or removal of atmospheric mass at the surface over the poles. As such, eliminating the condensation flow in the model requires eliminating these gradients by switching off the mass exchange with the surface. We do this in the model by allowing the surface model to gain and lose CO_2 ice (thus generating a seasonal cycle of surface ice deposits), while disallowing the mass exchange with the atmosphere (i.e., the model no longer conserves total CO_2 but does conserve atmospheric CO_2). Thus we not only eliminate the condensation flow but also the seasonal pressure cycle.
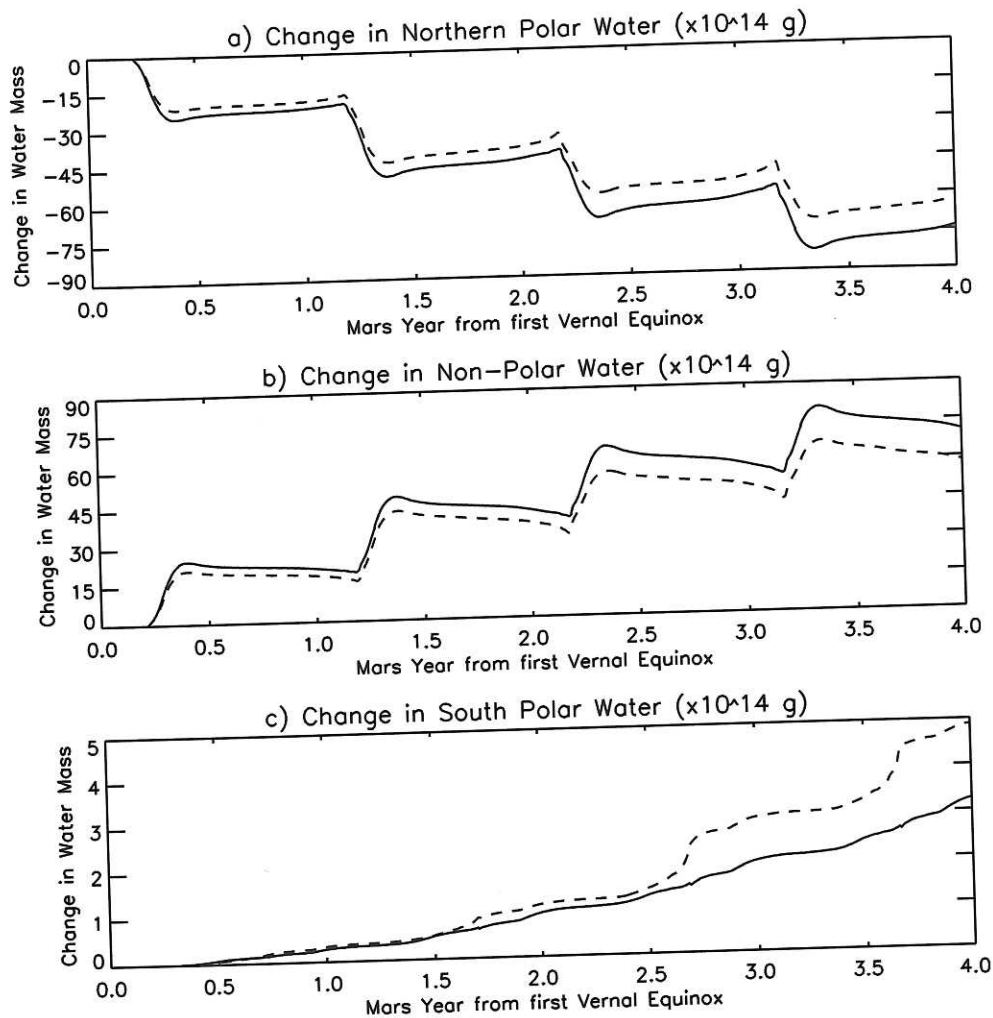
[53] The net flow of the atmosphere from pole-to-pole has been suggested as a mechanism for providing a bias in interhemispheric water transport. The southern summer return flow is stronger than its northern counterpart due to the more extensive southern winter seasonal cap. Thus this flow may explain the maintenance of an annual-average bias in water vapor, with the northern hemisphere being wetter [*James and North*, 1982]. Whether such a gradient in annual-average water vapor really exists in the Martian atmosphere is unclear given the nature of the southern summer observations.

[54] Figure 11 shows modeled water cycles with the condensation cycle switched on and off. The control simulation (the "on" case) is the ES simulation from section 3. In both cases, the output come from the fourth year of simulation, before the model has reached steady state, so the output should be used only to gauge relative differences between the models. It is clear from Figure 11 that the control simulation is able to generate larger vapor columns in both summer polar regions than the no-CO_2-flow case. The control is in general wetter.

[55] The variations in surface pressure are shown in Figures 11c and 11d for the two simulations. The double-peaked behavior of the control simulation (with peaks in
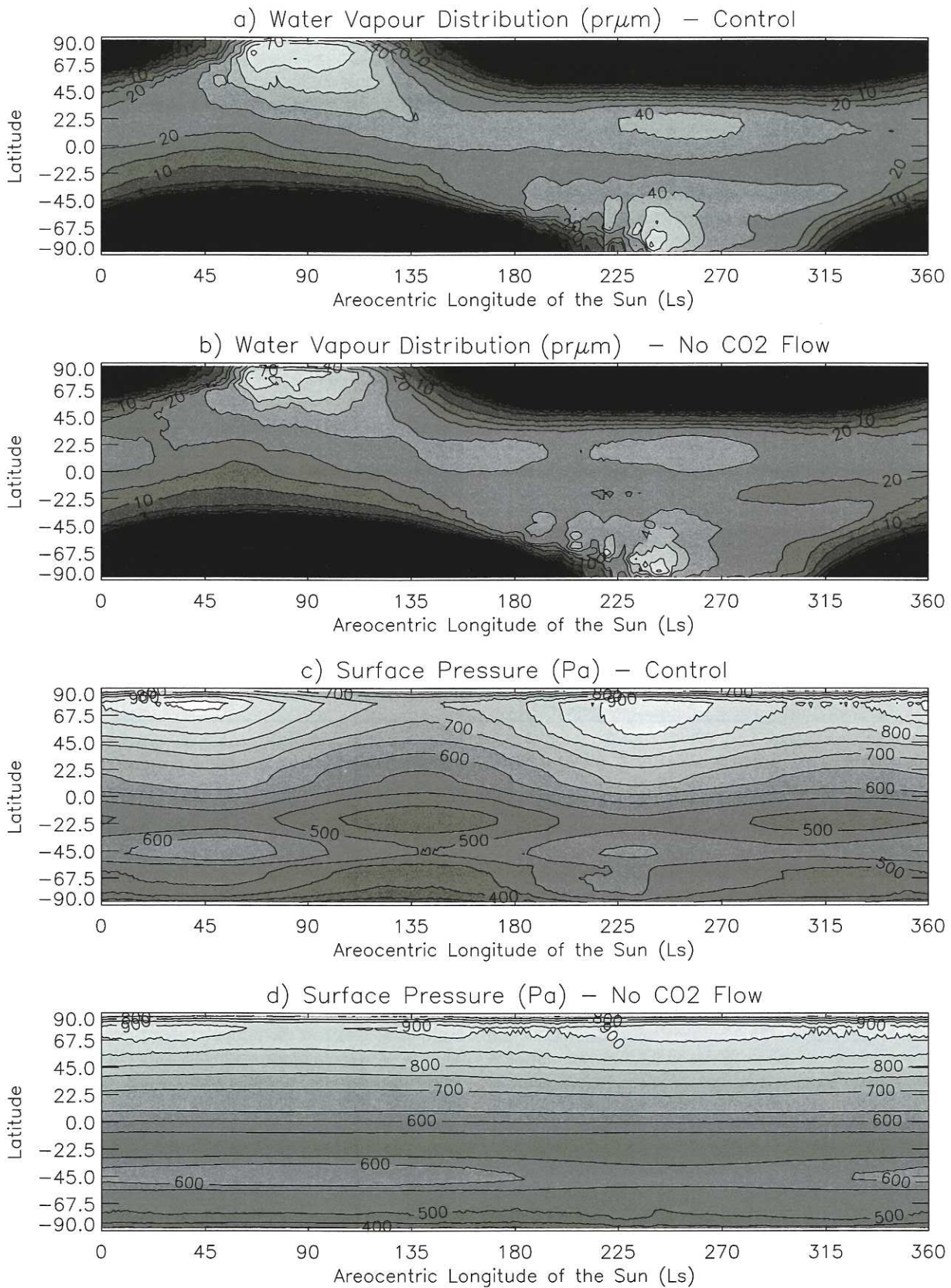
Figure 11. (a, b) Water vapor and (c, d) surface pressure output for a control simulation (the VS case) and a simulation in which the atmospheric pressure is not modified by sublimation or condensation of CO_2 ice ("No CO_2 Flow" case). The vapor distributions are of the same format as Figure 4a. The pressure is shown in units of Pascals and linearly contoured in steps of 100 Pa.

a) Change in Northern Polar Water (x10^14 g)

b) Change in Non-Polar Water (x10^14 g)

c) Change in South Polar Water (x10^14 g)

Figure 12. Change in the budgetary elements defined in Figure 6 for (solid) the control (VS) case and (dashed) the "No CO_2 Flow" case. "Nonpolar water" corresponds to "All other system water" in Figure 6.

spring in both hemispheres) reproduces the Viking Lander surface pressure observations, with a constant offset (discussed in section 3). The higher vapor loads in the control simulation at both polar solstices are not related to differences in total mass over the poles, as these are quite similar in the two simulations. The higher vapor loading in the control simulation in the northern tropics in late northern summer is also clearly not related to total column mass, as the no-CO_2-flow simulation actually has higher surface pressures at this time. Thus differences must be more closely associated with transport.

[56] The budgets for global water, defined in section 3 and in Figure 6, are shown in Figure 12 for the two simulations. Four years of output, which is as far as the no-CO_2-flow simulation was run, are shown. It is clear from Figure 12a that the control simulation is able to export much more water from the northern polar column than in the no-CO_2-flow case. Closer examination of Figure 12a shows that the nonsummer return flow is very similar in the two models, with the divergence between the lines occurring primarily due to higher summer time export fluxes in the control simulation. Since the majority of this flux occurs

after the northern seasonal ice cap has been removed, this greater transport flux is presumably driven by the draw-down of CO_2 in the southern polar regions. The greater export of water from the northern polar regions with the condensation flow active is also reflected in the more rapid condensation flow active is also reflected in the more rapid buildup of water in the nonpolar atmosphere (Figure 12b). This is also consistent with the generally higher global vapor amounts seen in the control simulation atmosphere in Figure 11. These results suggest that the net effect of the condensation flow is to inject more water into the global system from the northern polar source than would occur in its absence. It certainly does not seem to be the case that the transport of water into the northern polar regions during the nonsummer periods is greatly increased by the presence of a condensation flow. These results therefore do not support the suggestion of *James* [1985]. As to whether there remains a difference in the global vapor distributions between the two cases at steady state remains uncertain as the no-CO_2-flow case was not run to equilibrium, in part because the simulation already clearly showed that the CO_2 flow is not providing an important contribution to limiting vapor to the northern hemisphere.

[57] Figure 11c shows one final, interesting behavior in the no-CO_2-flow simulation. The non-CO_2-flow case is able to trap much more water on the southern residual ice cap than is the control case. The primary difference in water accumulation behavior is the rapid pulse of water into the cold trap just before southern summer solstice. This timing is coincident with the arrival of the wet seasonal cap edge at high southern polar latitudes (see section 3), which is the source for vapor in the atmosphere in the southern summer polar regions. In the control simulation, much of this water is moved by the condensation flow away from the cap and into the global water system. In the no-CO_2-flow case, there is less off-cap transport, and thus more water is left in contact with and is lost to the southern residual ice cap.

5. Importance of the Regolith

[58] All of the simulations discussed to this point have neglected the regolith as an active water reservoir. By the regolith reservoir we mean a site for water storage that is in diffusive contact with the atmosphere (through cracks and interconnected pores in the subsurface), which provides water storage through the physical binding of water molecules to the material constituting the pore walls of the subsurface (the regolith), i.e., adsorption of water to the material composing the near subsurface. This reservoir should exchange water with the atmosphere as the temperature of the subsurface changes and as the amount of water vapor in the near-surface atmosphere changes. Thorough descriptions of the adsorption process, applicability to Mars, and inherent uncertainties are provided by *Jakosky* [1985] and *Zent et al.* [1993].

[59] We have already shown, in section 3, that the GCM model of the water cycle without a regolith will come into approximate equilibrium (minus the small net loss to the southern pole) with global water amounts within a factor of 2 or so of those observed, at the same time producing a temporal and latitudinal vapor distribution that is in good qualitative agreement with observations. However, one can ask two important questions at this juncture: First, why is the model too wet (why does it over predict global vapor amounts)? Also, more fundamentally, what is the role of the regolith if it is not a central factor in stabilizing the water cycle?

[60] In this section, we seek to answer the second question. A priori, one might also expect that inclusion of an adsorbing regolith might provide a mechanism to reduce the amount of vapor in the atmosphere (directly or by limit transport away from the northern polar regions). We investigate these questions in this section by including a simple regolith adsorption scheme in the GCM water cycle.

5.1. Regolith Adsorption Scheme

[61] In this study, we use a slightly adapted version of the two-level regolith exchange model developed for use in circulation models by H97. While more detailed schemes for vapor diffusion through and water storage in the regolith have been developed [*Zent et al.*, 1993; *Mellon and Jakosky*, 1993], such schemes provide a level of complexity incommensurate with the rest of this study. The simpler two-level model of H97 was developed using results from *Zent et al.* [1993] and subsequent studies by Zent and

coworkers and captures, at a more crude level, the fundamental behavior of these more complex models.

[62] The two levels in the H97 scheme comprise an upper regolith layer of roughly the thickness estimated to be in diurnal communication with the atmosphere ($\sim$1 cm), and a thicker, lower level, which is estimated to exchange on 100-day timescales ($\sim$10 cm). In the H97 implementation the uppermost level is assumed to be in instantaneous communication with the lowest atmospheric level. This is justified by the lack of a diurnal cycle in the H97 model. At any given time step in the H97 adsorption scheme the total water in the lowest atmospheric level and the upper regolith level is summed, and then repartitioned so that the regolith comes into equilibrium with the new vapor abundance. Only if the atmosphere and regolith become saturated is ice formed. Exchange between the two regolith levels occurs through diffusion with a time-scale of 100 days (i.e., if the reservoirs are otherwise unaltered, they will equilibrate from any given initial distribution in 100 days).

[63] When implemented in this manner in the diurnal cycle-resolving Mars GCM, we have found that the resulting diurnal cycle of vapor in the lowest model level becomes excessively large when compared with the more accurate *Zent et al.* [1993] model. The reason for this is that the H97 scheme is designed to capture the effects of full, midday ventilation of the boundary layer (in the H97 model this mixing occurs up to a prescribed level, roughly 3.5 km above the surface). However, during the night the real boundary layer will collapse as a near-surface inversion develops in response to strong surface cooling, and this will greatly reduce the depth of mixing [e.g., *Stull*, 1988]. While this is not a concern for the H97 diurnal average model, we must account for it. In essence, by applying the H97 regolith scheme as is, we were unphysically allowing the upper regolith layer to be in instantaneous exchange with the atmosphere, rather than there being a 1-day time constant.

[64] In order to represent the effects of diurnal variability in vertical mixing to or away from the surface, we take the following approach to the implementation of the coupled regolith-boundary layer scheme. When surface temperatures exceed those of the lowest atmospheric level, the fully ventilated H97 scheme is activated and continues in this state until surface temperatures begin to decrease in the afternoon. For the rest of the diurnal cycle we use a scheme that restricts exchange with the regolith. We recast the scheme to use the boundary layer source flux equations used to treat release from surface ice deposits [*Ingersoll*, 1970]. From the adsorbed water amount we calculate the equilibrium vapor amount for that deposit. Any difference between this amount and the vapor in the lowest atmospheric level is used as the source strength in the exchange scheme. Regardless of whether the time of day dictates the use of the *Ingersoll* [1970] exchange equations or free ventilation, if the regolith and lowest atmospheric level become saturated, any additional water is converted to ice which is assumed to exist at the surface (thus we do not treat subsurface ice). Once formed, the surface ice cuts off exchange between the atmosphere and the subsurface, and communication with the subsurface is only resumed once all of the surface ice
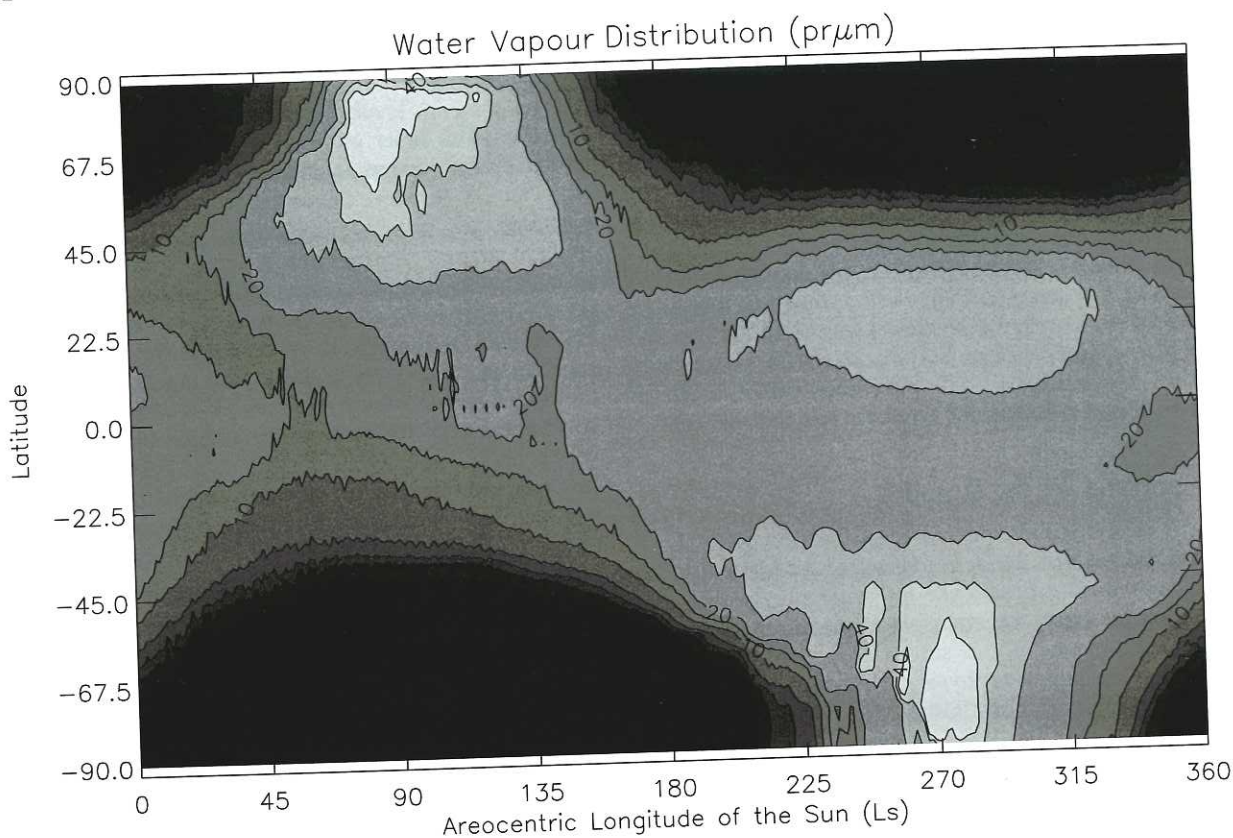
Figure 13. Same as Figure 4a but for the active regolith (RA) simulation.

has sublimed. The results of this scheme for idealized cases compare well with those of *Zent et al.* [1993].

5.2. Active Regolith Simulations

[65] The key tunable parameter in the H97 regolith scheme is the epsilon parameter ε, which captures all of the uncertainties in regolith adsorptive strength and physically associates them with subsurface pore space area. The larger the ε, the stronger the regolith adsorption. H97 find that with a value of $\varepsilon = 1$, which corresponds to the adsorption parameters of *Fanale and Cannon* [1974], the global model is desiccated: the water has been almost fully taken up by the regolith.

[66] Figure 13 shows the latitudinal and seasonal distribution of water vapor in the Mars GCM with active regolith after 6 model years. Although the model is not yet at equilibrium, the simulation was started with a desiccated atmosphere and was continuing to accrue water vapor when terminated. In fact, the regolith-active simulation (RA) at 6 years has higher water vapor than the inactive-regolith control (the VS simulation from section 3) at 9 years (compare Figure 13 with Figure 4a). Simulations with lower ε values show similar results, but with slower vapor accumulation times.

[67] Figure 14 shows the water budgets for the regolith simulation (RA) directly comparable with those for the VS simulation shown in Figure 5. Comparison of the first panel from both Figures 5 and 14 shows that the RA simulation is much more effective at building up vapor amounts in both hemispheres. By year 6 the RA case contains over 20% more vapor than the VS simulation. A key reason for this is

that the RA simulation moves substantially more water between the hemispheres each year than does the VS simulation (cf. Figures 14b and 5b). How is this happening? One could suggest that the regolith is simply outgassing vapor that is accumulating in the RA simulation atmosphere. However, the regolith was initialized as desiccated in the RA simulation. Indeed, the regolith is clearly gaining water from the system as can be seen in Figure 14d, where the "nonpolar water" budget excludes regolith water. The northern polar water budget is decreasing faster than the other two budgets are increasing. At the end of the sixth year the northern polar cap has released roughly 6×10^{14} g more water than the southern pole or all other nonregolith reservoirs have accrued.

[68] Our interpretation of these results certainly includes the conclusion that the regolith does not provide a strong desiccating buffer for the water cycle. For values of epsilon that produce a dry atmosphere in the H97 model, we find a small increase in the global vapor abundance. This result originates from the same model bug found in the H97 work discussed in sections 1.1 and 3.3. For this reason, we believe the large-scale picture of the water cycle and the involvement of the regolith, as described in that work, is wrong. The reason that the atmosphere becomes more moist in the RA simulation despite the fact that the regolith is actively accruing water is that the regolith acts as an additional communicative site for water outside of the northern polar cap. As such, it can effectively decrease the amount of water available to be taken into the northern polar region outside of northern summer and act to effectively decrease nonpolar water during summer. Early in the simulation, the regolith
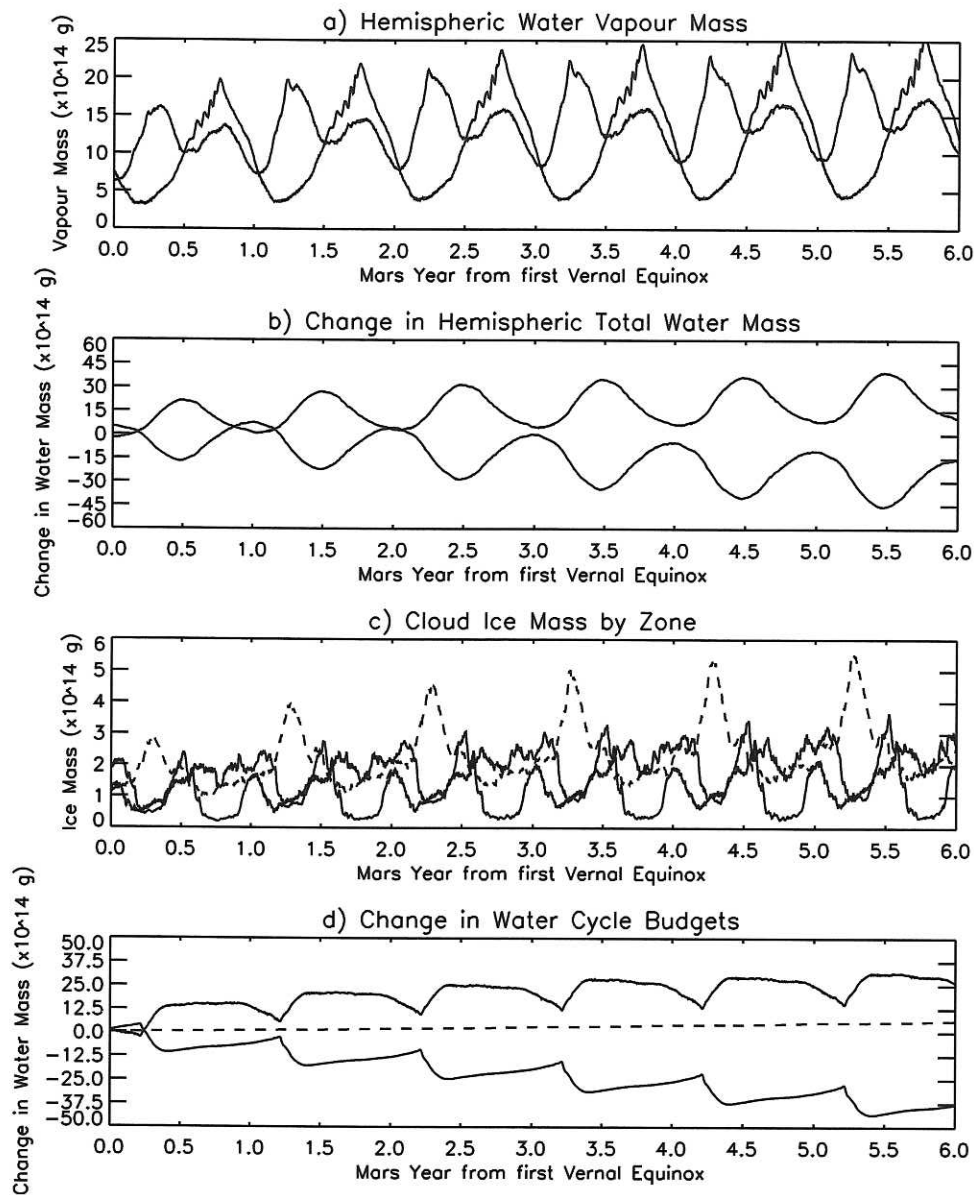
Figure 14. Same as Figure 5 but for the active regolith (RA) simulation.

operates in both ways. As the regolith fills and the atmosphere becomes more moist, it loses the ability to enhance northern summer outflow. This serves to decrease return flow influxes to the northern cap and to increase northern summer outflow of water. Within the context of the water cycle equilibration process outlined in section 3, both of these effects will tend to increase the amount of water outside of the northern polar region. Comparing Figures 13 and 4, it is clear that the regolith acts to redistribute water vapor relative to a nonregolith simulation. It is also seems conceptually likely that the regolith will slow the whole equilibration cycle, as water moves between regolith sites at different points on the planet, although much longer simulations are required to assess the validity of this statement (it is not proven here). Interestingly, given the fact that the regolith allows a continuum of exchange time constants, the regolith will contain a "memory" of water behavior, and it is possible that interannual variability may result from putative

oscillations in this system. Further work on the behavior of the regolith within the context of a complete GCM water cycle model is necessary.

6. On the Stability of a Southern Polar Water Ice Cap

[69] In section 3 we examined the mechanisms controlling the model seasonal water cycle and found that the northern cap temperature sets the steady state global vapor abundance, given a repeatable annual cycle of atmospheric mixing vigor. The steady state is maintained owing to the separation of variables controlling the flow of water into the northern polar region in autumn, winter, and spring, and those controlling the flow out of the northern cap during northern summer. An interesting question then presents itself in the form: What would happen if both the northern and southern caps were to be free of CO_2 ice every summer?
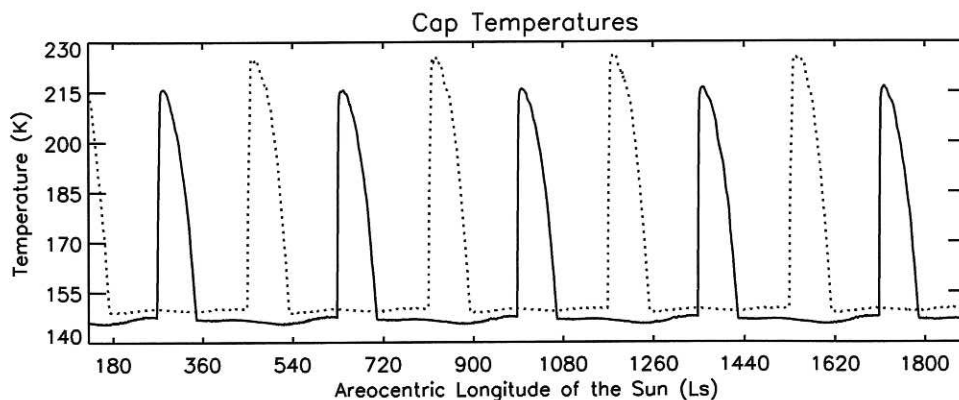
Figure 15. Model northern and southern polar cap surface temperatures (averaged within 10° of the pole in each case) for a simulation in which no CO_2 residual ice cap is prescribed at the southern pole and water ice residual caps are defined at both poles. Northern cap temperatures are defined by the solid line, while southern cap temperatures are defined by the dotted line. Note that the southern cap albedo and thermal inertia have been defined so as to limit the peak southern cap temperatures to be lower than those of the north (see text for discussion).

The discussion above shows that the northern cap "seeks" an equilibrium vapor amount (by driving toward an annual average zero flux across the polar boundary), and it should be expected that the southern cap would behave likewise. This suggests that the two caps will compete for the water, and that in this way, water may only be "stable" at one pole. In this section, we address the question of differential cap stability by allowing exposed residual water ice caps at both poles during their respective summers and tracking the net interhemispheric transfer of water. While the results presented here cannot be considered conclusive, they suggest that asymmetries in atmospheric transport and surface thermal environment conspire to make the northern pole the preferred location for water within the current orbital state.

[70] In conducting this experiment we face an important obstacle: we do not know the albedo, thermal inertia, or extent of the hypothetical southern water ice cap. For the purposes of this experiment we assume southern cap properties such that the southern cap center temperature at its peak is less than the northern cap center temperature at its peak

(Figure 15). This is done to preferentially stabilize the southern cap, all else being equal. The simulation is begun from the "cool, wet" (CW) case, discussed in section 3, after 3.75×10^{14} g of water ice have accumulated in the region south of 75°S, with over 1.5×10^{14} g of this on the southernmost grid point. Otherwise, we use the same model setup as used in the CW case.

[71] The chosen cap properties result in the southern cap subliming less vapor than the northern cap despite higher insolation during southern summer. Figure 16 shows the vapor mass north of 60°N and south of 60°S for the duration of the simulation (almost 5 Mars years). Thus the southern cap provides less of a vapor-gradient drive for transport, and when combined with the shorter southern summer, suggests that the south cap ought to be less efficient at exporting vapor. Additionally, both hemispheres show decreasing vapor abundances, confirming the fact that the CW simulation is over initialized with vapor.

[72] The model budgets of vapor, surface ice, and cloud ice are shown in Figure 17. There is a clear anticorrelation
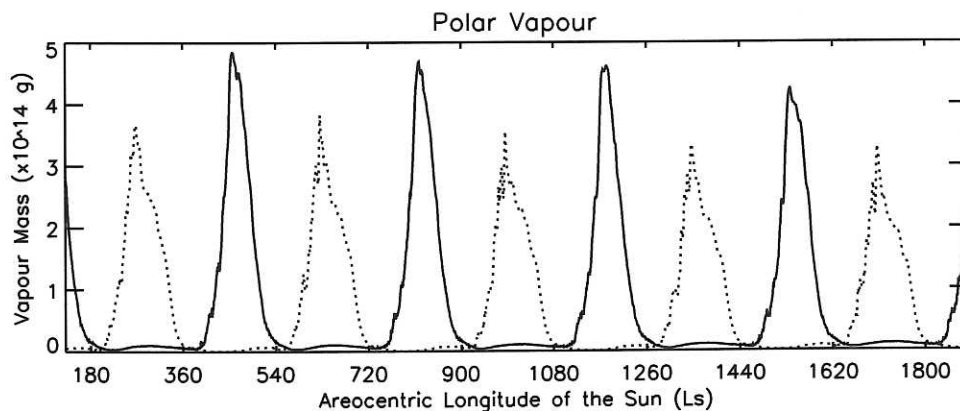
Figure 16. The mass of water vapor in the polar regions of both hemispheres for a simulation with two active residual water ice caps. The solid line corresponds to vapor between 60°N and the north pole, while the dotted line corresponds to vapor between 60°S and the southern pole. Corresponding cap temperatures are shown in Figure 15.
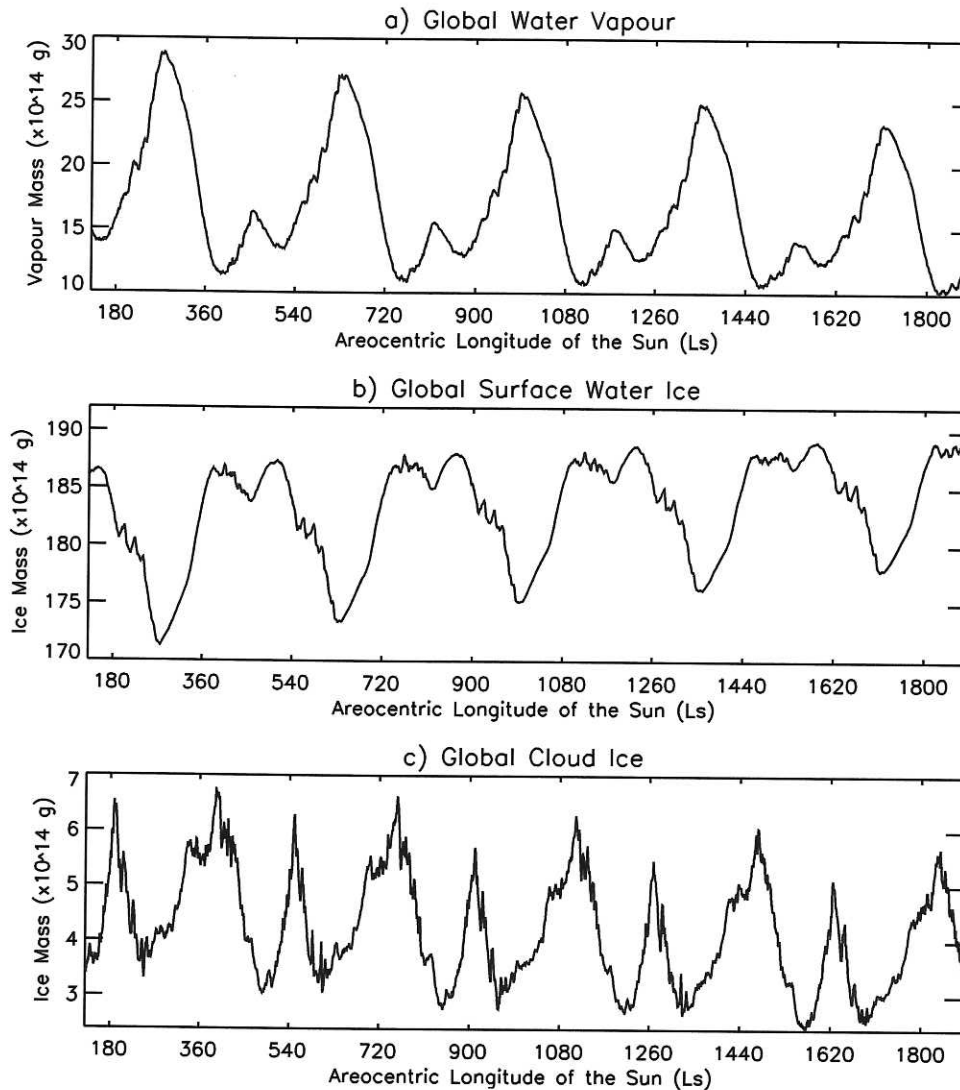
Figure 17. Same as Figure 3 but for a simulation with two active residual water ice caps.

between surface ice and vapor. The largest swing between these reservoirs occurs during southern summer as water exchanges between the southern seasonal ice cap and the atmosphere. The northern summer exchange is much smaller, resulting mainly from the difference in insolation between the two seasons. As the model runs for several Mars years, the total surface ice inventory increases at the expense of atmospheric vapor. Cloud ice mass holds at a steady annual average fraction of vapor (~25%), with cloud preferentially forming during early spring and late summer in each hemisphere. Thus, as the total vapor amount decreases through the simulation, so does the amount of cloud ice.

[73] The relative effectiveness of the two caps is not clear from the preceding figures. Again, we will use the reservoirs defined in section 3 and Figure 6. Figure 18 shows the model evolution of northern polar column water (vapor, cloud, and surface ice north of 75°N), south polar cap ice (surface ice south of 85°S), and all other system water. We use only the surface ice at the southern cap center because the evolution of this budget alone readily indicates whether the southern cap is gaining or losing water. If this budget

continually increases, the southern cap is stable. However, if it loses mass and eventually sublimes, the southern cap is not stable. Figure 18 shows the model southern cap sublimes away as a function of time while the northern polar region accumulates water. The final midsummer dip in ice abundance at the south pole depletes the southern ice mass to roughly 10% of its original mass and had the simulation continued for an additional year, the southern cap would likely have vanished.

[74] That our results for the southern cap are not biased by the different definitions of northern and southern polar water used in Figure 18 is demonstrated by Figure 19. Here, the total water mass (vapor, surface ice, and cloud ice) in each hemisphere is plotted as a function of time for the duration of the simulation. The northern hemisphere is clearly accumulating water at the expense of the south.

[75] These results suggest that both atmospheric transport and surface thermal environment may contribute to make water unstable in the southern hemisphere, either as surface/subsurface ice or as adsorbed water in the regolith, for the current orbital state. It is important to note that we can only discuss water in the uppermost part of the subsurface, that
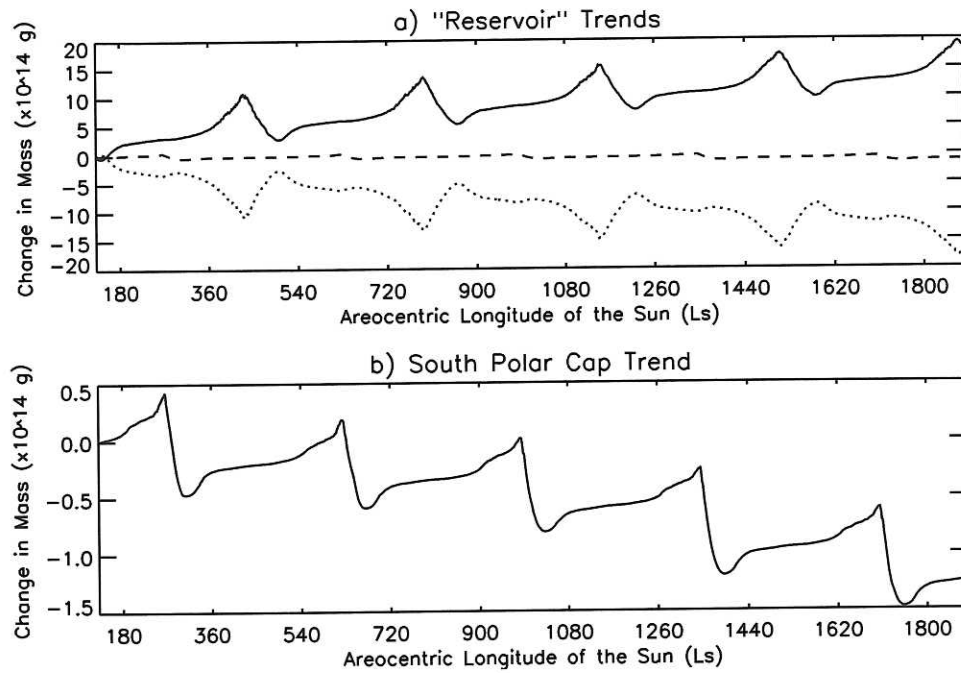
Figure 18. The evolution of water budgets defined in Figure 6 for a simulation with two active residual water ice caps. (a) Solid line is northern polar water, dashed line is southern polar cap water ice, and dotted line is all other water. (b) Expansion of dashed line in Figure 18a.

part that exchanges on timescales of less than a few thousand Mars years. Far more importantly, we must be extremely cautious in discussing these results because of their dependence on the validity of the transport model, the validity of surface vapor flux dependence on surface temperature, and our use of only surface ice reservoirs. The reason for the northern bias in stability, even when the cap thermal environments are biased for southern stability, are beyond the scope of this paper, but we suggest that they are related to the findings of *Fenton and Richardson* [2001] and *Richardson and Wilson* [2002] that the annual average Hadley circulation is biased in favor of the southern summer circulation. Further, this bias is not related to the argument of perihelion [*Fenton and Richardson*, 2001], but to the center-of-mass/center-of-figure offset of the planet [*Smith and Zuber*, 1996].

Such a suggestion could "easily" be tested (it is "easy" but not easy owing to the CPU time required) by conducting multiannual simulations with topographic variations removed or the current topography switched with the south being the lower hemisphere. In each of these cases, the evolution of the water cycle could be monitored. In any case, this requires further study, but we suggest here that cap stability defined as above may be a fundamental outcome of large biases in planetary topography.

7. Water Cycle at High-Obliquity and the "Stability" of Equatorial Ice

[76] A significant reason for developing a mechanistic model of the Martian water cycle is the desire to use such
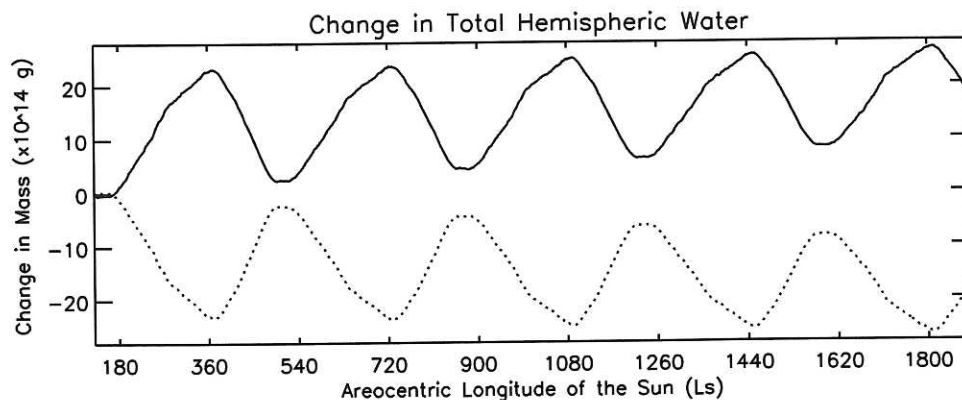
Figure 19. The evolution of total water substance in each hemisphere for a simulation with two active residual water ice caps. Solid line is northern hemisphere water, while the dotted line in southern hemisphere water.
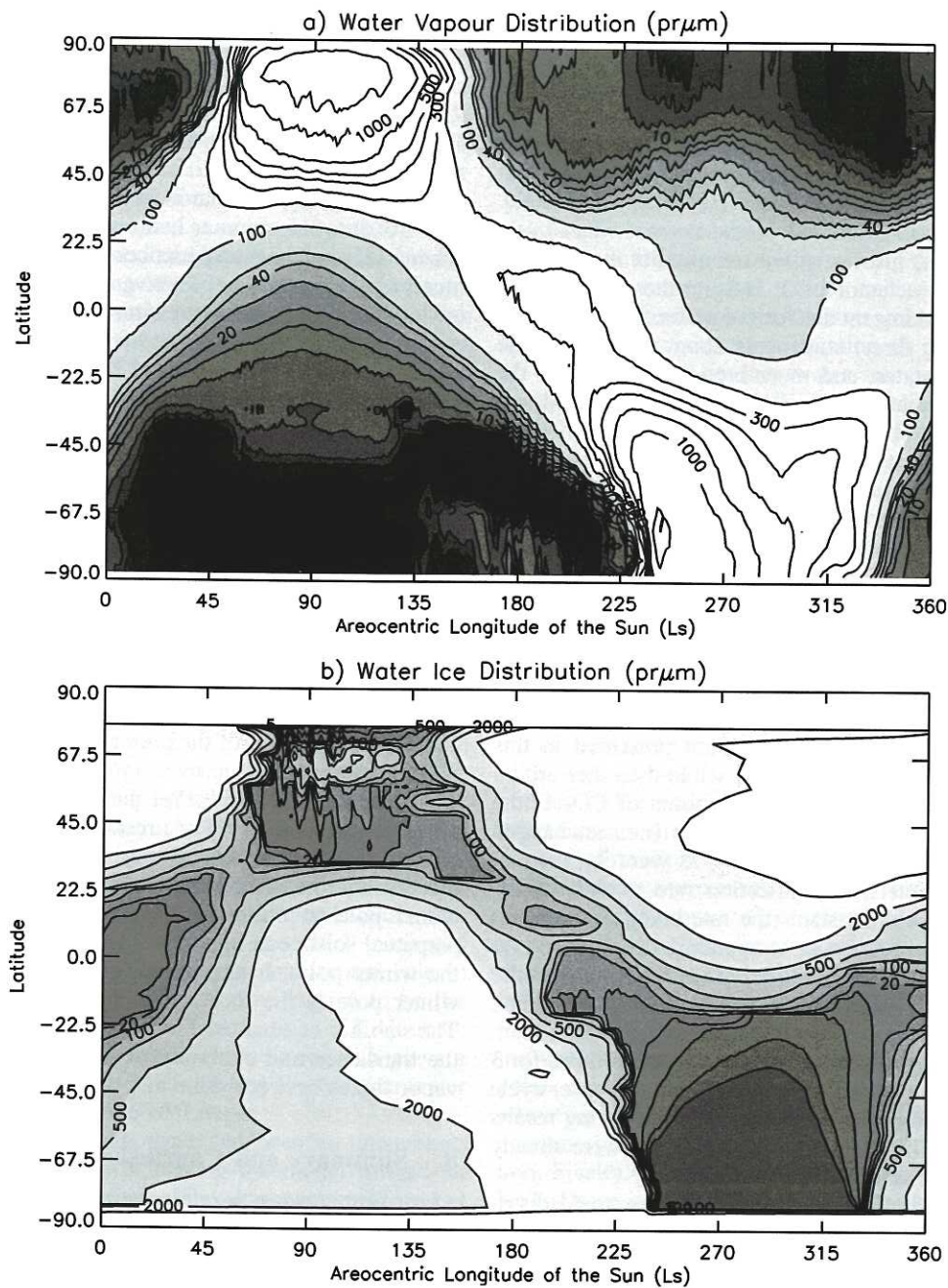
Figure 20. The latitudinal and seasonal evolution of zonal average (a) water vapor and (b) surface water ice for a simulation in which the planetary obliquity is increased from 25° to 45°. The annual cycle comes from the third year of the simulation (the simulation was begun with a dry atmosphere and water ice only north of 80°N). Note that the maximum vapor contour is 2000 prμm, while the maximum ice contour is 3000 prμm.

a model in addressing questions of how the water cycle might have behaved at times when the forcing or boundary conditions were significantly different than we find them today. An interesting example of such a paleoclimate question for Mars is that of the behavior of the water cycle when the planetary obliquity, or tilt of the rotation axis relative to the orbit plane normal, was high. Over the course of the past few millions of years the highest value that the obliquity of Mars is expected to have reached is ~45°. While it is possible that obliquities as high as 60°

may have obtained at some point in the more distant past, the 45° case provides a nice upper bounds for simulations in which we can be reasonably confident that available volatile inventories were not greatly dissimilar from those of today. Of course, there are many uncertainties in modeling Martian paleoclimate. The degree to which the ambient atmospheric pressure will rise at high obliquity is not particularly well understood, though models of regolith interaction suggest that only a factor of 2 or so should be expected [*Zent and Quinn*, 1997]. The thermal and albedo

behavior of CO_2 ices comprising the polar caps is not well understood [*Kieffer et al.*, 2000], with much variability exhibited, including an indication that albedo and insolation are coupled [*Kieffer and Zent*, 1992]. We do not understand the coupling between the circulation and dust injection that can significantly alter the bulk transport capacity of the atmosphere [e.g., *Zurek et al.*, 1992]. Closer to home, our emulation of the current water cycle is far from perfect, insofar as we overpredict water vapor amounts by up to a factor of 2. Despite these limitations, we do have a working model for the water cycle which is capable of making direct statements about the water cycle for other forcing states, and more broadly, a model of the circulation and climate which is both physically based and well tested against observations. In any case, it is interesting to examine what these models suggest about paleoclimate, if only to understand how these predictions change as the incorporation of increased understanding progresses (to understand how globally important those elements of increased understanding really are). As a starting point for the investigation of paleoclimate with Martian GCM systems, we present the case of the water cycle at 45° obliquity, and specifically investigate the case of surface water ice stability at the equator, as suggested by *Jakosky and Carr* [1985].

[77] For the high-obliquity simulation presented in this section, the obliquity was set to 45° while the other orbital parameters were held constant. The amount of CO_2 in the atmosphere/ice system was held constant (i.e., unchanged from the current climate simulations), as were ice thermal and optical parameters. The injection rate of dust at the surface was also held constant (the rate being the same as that necessary to reproduce air temperature observations for the current climate). The model does not include the radiative effects of water vapor or ice in the atmosphere, or the latent heat effects of water condensation/sublimation. The model was begun from a dry atmosphere and run for 3 Martian years. We stopped the model before the water cycle had come to equilibrium, in part because interesting results regarding the stability of equatorial surface ice were already clearly apparent after a few model years.

[78] Figure 20 shows the latitudinal and seasonal distributions of atmospheric water vapor and surface water ice for the third year of model integration. It should be noted that the global water vapor was still increasing quite strongly at this point in the simulation (as would be expected from the estimation in section 3 for an equilibration time constant of roughly 10 or so Mars years). Despite this, the atmosphere is already extremely wet, producing peak northern hemisphere summer water amounts of over 2000 prμm (Figure 20b). Peak water amounts in both hemispheres occur in the polar regions. In the north the water comes from the residual cap. In the south the water comes from the subliming seasonal ice cap (the "quasi-solid-state" transport of water along the cap edge, described in section 3, is highly active in concentrating water ice near the pole late southern spring, see Figure 20a). It should be noted that the peak water amounts in the southern hemisphere are much shorter lived and more latitudinally constrained than in the north. In this simulation, the northern hemisphere is much wetter than the south, unlike our standard climate simulations. However, this may be a product of nonequilibrium.

[79] The important result of this simulation with respect to simpler model predictions of stable equatorial surface ice is shown in Figure 20a. The behavior of the seasonal ice deposits is qualitatively very similar to that for the current climate, save for the fact that the water component is much more latitudinally extended. The southern hemisphere seasonal ice cap in particular is extremely extended, reaching over 30° into the summer hemisphere. The northern hemisphere seasonal cap experiences a shorter winter with a much weaker vapor source active in the summer hemisphere (at least at this stage of the simulation). Even so, the cap extends over the equator. Another band of ice occurs in the high latitudes of the northern hemisphere during northern summer. This ice is precipitated from and stabilized by the very high vapor column over the pole (and where it meets slightly cooler, more southerly air).

[80] Figure 20a shows that ice does not so much become stable at the equator as the seasonal ice caps become so extensive in the face of much higher atmospheric vapor loads that they run into each other near the equinoxes. This is, of course, a purely semantic point. Thermodynamically (if not dynamically) the overlapping seasonal caps are identical to the statement that ice is stable year-round at the equator (note that this result differs from that of an earlier report [*Richardson and Wilson*, 2000] due to the complete exhaustion of the prescribed northern polar cap in that simulation). In fact, ice is most stable between 10° and 20° north of the equator. Yet the model shows that this is physically accomplished as a residual of very large fluxes of water between the hemispheres. At any given point, the place where the equilibrium vapor pressure is lowest is the winter pole (if one were to artificially lock Mars into a perpetual solstice at high obliquity, water would migrate to the winter pole). In this sense, even at high obliquity, the winter pole is the most "attractive" place for water ice. The stability of equatorial ice at high obliquity is a result of the transience and extremity of the solstices and the large vapor fluxes between the two.

8. Summary and Conclusions

[81] In this paper, we describe results from the first effort to study the Martian water cycle with a full general circulation model. We concentrate primarily on elucidation of the primary mechanisms responsible for generating the observed cycle, and specifically those mechanisms primarily responsible for driving the cycle to an interannually repeatable steady state. We do not spend a great deal of effort "tuning" the model to provide a high precision emulation of the observed water cycle due to concerns over the accuracy of currently available water observations, the sensitivity of the details of the modeled water cycle to small errors in circulation and hence transport, and the fact that expenditure of laborious effort to "fit" the water cycle does not necessarily guarantee insight. Instead, we chose to concentrate on examining the qualitative fit of the model to observations, and more importantly, examining the water cycle system evolved by the model. We ask first order questions regarding the importance of surface ice deposits, seasonally varying transport modes, the condensation cycle of CO_2, and the regolith as an adsorbate reservoir for water. In developing a mechanistic model for the water cycle we

ask some preliminary questions regarding the differential stability of water ice at the two poles, and the behavior of surface ice deposits at higher obliquity. The latter are seen as prototype calculations suggesting the role of GCM models in addressing paleoclimatic questions for Mars, following the lead of terrestrial modeling.

[82] At a qualitative level the latitudinal and seasonal distribution of water vapor generated by the model (Figure 4a) provides a good emulation of the actual cycle, as observed by the Viking MAWD instrument (Figure 1). This emulation results despite the simplicity of the water cycle physical processes and the lack of an active (diffusing and adsorbing) regolith. The maxima in water vapor at the summer poles at both solstices are reproduced, as is the secondary maxima in water vapor in the northern tropics during northern winter, which is evident in the MAWD data, but has never before been captured in a model (cf. Figures 4a and 1). Despite the good "pattern fit" to the latitudinal and seasonal distribution, the model water cycle is too wet, by a factor of ~2. This suggests that either there are processes missing from the model that trap water after it has left the northern polar cap or that limit the ability of the atmosphere to transport water away from the northern cap. One possibility relates to the excessive area of the northern cap in the model that results from the coarse (5° of latitude) resolution, which allows only two latitudinal grid points on the cap, and hence a cap uniformly covering the pole out to 80°N. The impact of this larger cap on sublimation fluxes must be assessed with higher resolution models (such as a mesoscale model centered on the cap) in the future.

[83] In spite of the overly wet nature of the modeled water cycle, the atmosphere is by no means flooded with water. This was a central finding of H97, and one which motivated a conclusion that the regolith played an essential role in limiting water vapor. That result is now known to be the product of an error in the H97 calculations (H. Houben, personal communication, 1999). Thus the regolith plays a much less significant role in controlling the Martian water cycle than suggested by the H97 paper.

[84] The emphasis of this paper has been on uncovering the mechanisms at work in driving the model toward an equilibrium state. In this way, the dominant mechanisms controlling the water cycle may be identified. We developed a new set of water cycle budgetary components, defined in Figure 6, which provide much clearer insight into the equilibration processes than that afforded by examination of such quantities as total atmospheric vapor. An initial finding, in line with most earlier work [*Jakosky and Farmer*, 1982; *Jakosky*, 1983b; *Houben et al.*, 1997], is that the model will never come to a true equilibrium as there is ongoing, irreversible loss of water to the southern pole so long as there exists a residual CO_2 ice cap that pole. Despite this ongoing loss the model will come to a steady state, in which the nonpolar water reservoir (see Figure 6) repeats the same annual cycle, with a small net annual loss from the northern polar column being balanced by a net annual gain at the southern pole. Loss rates from the northern pole are highly speculative but are of the same order as suggested by *Haberle and Jakosky* [1990], roughly 0.1–1 mm per year. For a cap of order 1 km thick this corresponds to complete transfer in 1–10 million years. However, the water ice would not full transfer from the south to the north. It seems

to us that at some point the water ice on the southern cap would become sufficiently thick that the CO_2 would be buried, radiatively disconnected, and that the CO_2 ice would be unable to buffer the water ice temperatures (further, buried CO_2 ice is unstable and will be lost to the atmosphere). At that point the situation would be transformed into one of a residual water ice cap at both the north and the south, which we examine and find unstable (see section 6 and below), the system rapidly moving the water back to the north. In any case, other factors, such as obliquity change will complicate the picture on timescales of 10^4+ years.

[85] The processes of equilibration are related to the ability of the atmosphere to mix water into and away from the northern polar cap and the sublimation capacity of the northern polar cap. It is instructive to examine the history of mixing from the northern cap. During late northern spring and summer the north polar region rapidly loses water to the rest of the system. This large flux is driven by very strong meridional gradients in vapor evident in Figure 4 (and in observations, Figure 1), since the northern summer polar circulation appears not to be especially vigorous [*Houben et al.*, 1997; *Richardson*, 1999], although significantly more vigorous than suggested by the 2-D model of *Haberle and Jakosky* [1990]. By late northern summer the northern polar vapor outflow is stemmed and reverses to yield a sharp, strong influx of vapor. The influx corresponds to relatively high northern polar vapor amounts and the onset of strong cooling in the northern polar interior. Northern polar westerlies reestablish at this season and instabilities on the newly developed front provide strong mixing of water back into the pole. As autumn proceeds, the polar vortex wall and accompanying eddies move equatorward and little water mixes very deeply into the polar regions beyond the vortex. This is represented by the flattening of the northern polar vapor inflow between $L_s = 200°$ and $L_s = 320°$. As spring arrives at the northern pole, the northern polar vortex contracts, bringing vapor and eddies within reach of the northern residual polar cap. In addition, some water is carried along the retreating edge of the seasonal ice cap through a process of continuing sublimation, poleward mixing, and recondensation. Finally, by mid-to-late northern spring, sufficient CO_2 ice has been removed from the northern pole for water ice to sublime once more, regenerating the northern spring and summer vapor gradient and outflow.

[86] Combining the behavior of vapor gradients and mixing capacity as a function of season, the following paradigm for the model water cycle develops. During summer the northern cap will export to the rest of the planet a fixed amount of water that to first order, is only dependent upon north polar cap temperatures. During the rest of the year the circulation returns to the north polar cap an amount of water that depends, again to first order, only upon the amount of water sitting in the tropical/extratropical atmosphere. This separation of dependencies means that if we overinitialize the model (or the atmospheric water amount is perturbed high by some process), the action of the strong nonsummer circulation on the polar/extratropical gradient of vapor more than compensates for the "fixed" summertime export of polar water by the action of the effectively "weak" mixing on the much larger gradient in vapor. Conversely, a low or dry initialization will lead to the polar water export overwhelming the nonsummer return flow.

This self-regulation mechanism is clearly evident in the behavior of the model water budgets shown in Figures 5d, 7, and 10d. By these means the model will supply polar water to the rest of the planet when underinitialized or perturbed low, and soak up water when overinitialized or perturbed high. The timescale of this equilibration mechanism will be related to the transport vigor, which is likely misrepresented by the model (as gauged by the overly wet nature of the simulations). However, e-folding timescales of order tens of Martian years seem likely.

[87] Additional simulations were conducted to examine the impact of the CO_2 condensation flow (the net pole-to-pole wind associated with condensation and sublimation of CO_2 in the two polar regions) and the adsorbing regolith on the water cycle simulated by the model and upon the mechanisms responsible for equilibration. Elimination of the CO_2 flow was found to result in a generally drier model atmosphere related to two main mechanisms. First, the draw-down of atmospheric mass by the condensing southern seasonal ice cap generates an effective north-to-south transport in the full model that serves to extract more water vapor from the northern polar region than occurs in the absence of the condensation flow. Second, the outflow of subliming CO_2 in late southern spring causes much of the subliming water ice from the seasonal cap to be transported equatorward and away from the southern residual polar cap. When the CO_2 cycle is eliminated, more vapor remains over the southern residual ice cap and becomes permanently trapped there following vertical diffusion to the surface.

[88] Inclusion of a regolith reservoir was found to increase the globally integrated vapor content of the atmosphere, further worsening the fit to observations, although the strength of the regolith adsorbtivity used in this study may have been unrealistically high. This result is also in marked contrast to that of H97, wherein an equivalent value of adsorbtivity resulted in a nearly desiccated atmosphere. However, we believe that this discrepancy is related to the same model bug in the H97 work that generated the conclusion that the regolith was necessary (at lower levels of adsorbtivity) to prevent flooding. Using the conceptualization of the water cycle delineated in the equilibration experiments, the regolith acts to moisten the model atmosphere by trapping more water outside of the northern polar cap than would occur in the nonactive regolith simulation. The regolith also acts to diminish the vapor available for return transport to the polar cap during the nonsummer period. In any case, the regolith does not significantly change the latitudinal and seasonal distribution of vapor and does not seem to be an important driver of the Martian water cycle. The simulation presented here shows a regolith steadily accumulating vapor and coming into balance with the imposed atmospheric vapor load determined by the northern polar cap source, as suggested by *Jakosky* [1983b]. One interesting aspect of the regolith is the continuum of interaction timescales corresponding to depth beneath the surface. This effectively allows a memory site for water exchange, in weak analogy to the terrestrial oceans, and hence the possibility for interesting interannual variations in water cycle behavior. This requires further research.

[89] The question of why the northern pole is associated with higher vapor amounts, and more fundamentally, why the northern pole is associated with a residual water ice cap, is a complex question potentially involving mechanisms related to determination of water and CO_2 ice albedos, orbital forcing, and topography. In this study, we focused on potential dynamical mechanisms affecting stability of water ice at the two poles, by prescribing water ice caps at both poles. Acknowledging that the shorter, hotter southern summer may bias water ice stability to the north, we contrived to produce a southern cap peak temperature lower than that at the north, providing a thermodynamic bias for southern polar water stability. However, we found that even in this case, the southern summer pole "wants" to establish an extrapolar vapor amount that is higher than that required by the northern cap, and hence sublimates. On purely dynamical grounds, a southern water ice cap would be unstable with respect to the north. We suggest that this bias may be linked to the finding of *Fenton and Richardson* [2001] and *Richardson and Wilson* [2002] that the southern summer Hadley circulation is dominant in the annual average and that this bias is directly related to the topographic dichotomy (the large difference between centre of mass and center of figure [*Smith and Zuber*, 1996]). This suggestion should be examined by simulating the water cycle with flat topography and with the topography flipped north to south. We would predict that all else being equal, the high pole will lose water to the low pole, and that with flat topography the poles will by dynamically equal.

[90] Our final simulation provided an example of the paleoclimatic applicability of a water cycle model. We simulated a water cycle for Mars with an obliquity of 45°, and examined the latitudinal and seasonal cycles of vapor and surface ice deposits. The much greater insolation at the poles was seen to generate very high water vapor amounts over the northern pole, exceeding 2000 pr μm. This higher vapor amount, combined with larger polar night regions and hence larger seasonal CO_2 ice caps, allowed much more extensive water ice caps. These caps were found to expand well into the summer hemisphere. Further, the caps were found to overlap in the northern tropics near the equinoxes, resulting in a band of permanent ice. Thus, while the winter poles remained the most "attractive" place for water at any given time (in the sense that the condensation point partial pressure is lowest there), ice remained stable near the equator year-round, as suggested by *Jakosky and Carr* [1985].
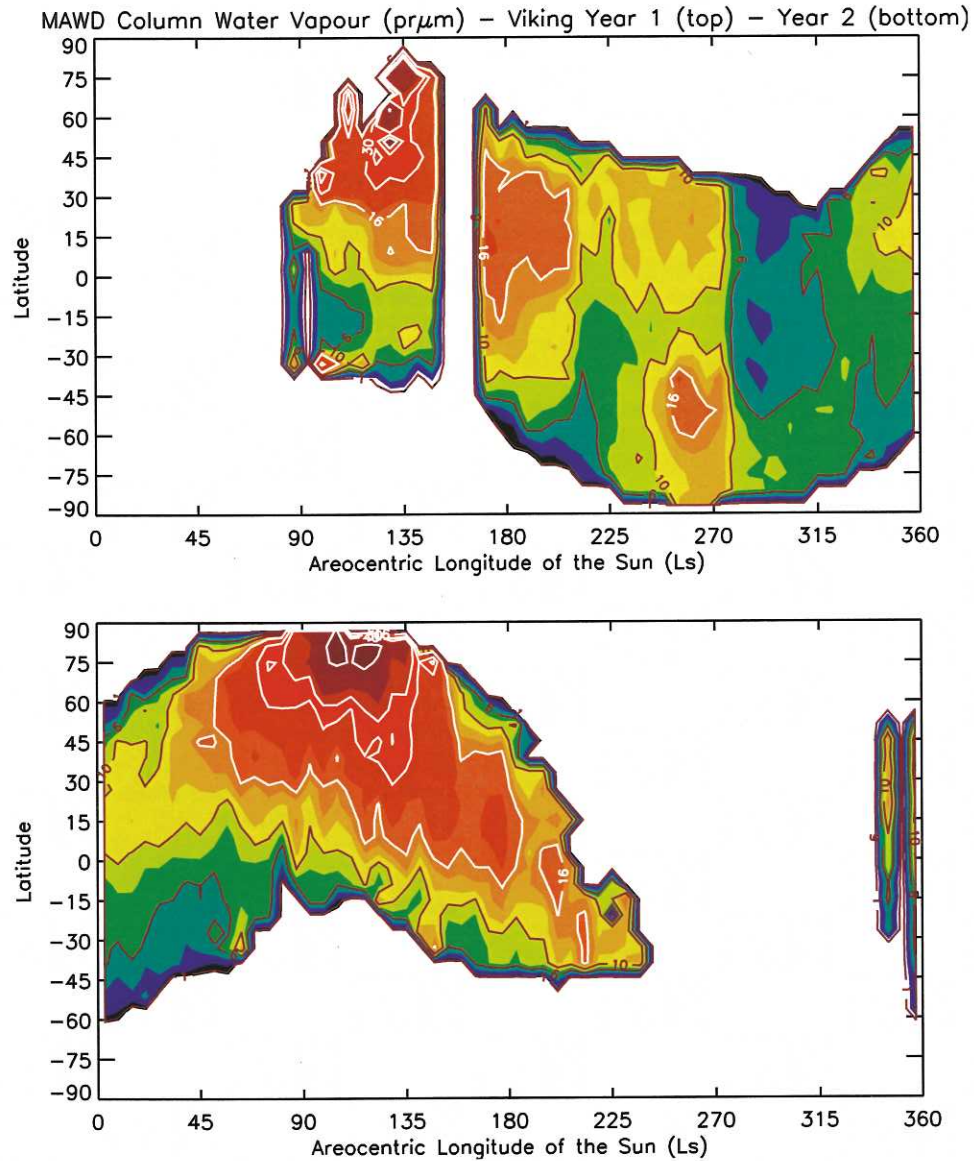
References

Baker, V. R., R. G. Strom, S. K. Croft, V. C. Gulick, J. S. Kargel, and G. Komatsu, Ancient oceans, ice sheets and the hydrologic cycle on Mars, *Nature*, *352*, 589–594, 1991.

Barnes, J. R., J. B. Pollack, R. M. Haberle, C. B. Leovy, R. W. Zurek, H. Lee, and J. Schaeffer, Mars atmospheric dynamics as simulated by the NASA Ames general circulation model, 2, Transient baroclinic eddies, *J. Geophys. Res.*, *98*, 3125–3148, 1993.

Bar-Nun, A., G. Herman, D. Laufer, and M. L. Rappaport, Trapping and release of gases by water ice and implications for icy bodies, *Icarus*, *63*, 317–332, 1985.

Briegleb, B. P., Delta-Eddington approximation for solar radiation in the NCAR community climate model, *J. Geophys. Res.*, *97*, 7603–7612, 1992.

Burk, S. D., Diurnal winds near the Martian polar caps, *J. Atmos. Sci.*, *33*, 923–939, 1976.

Clancy, R. T., Atmospheric dust-water interactions: Do they play important roles in the current Mars climate?, in *Workshop on Evolution of Martian Volatiles*, LPI Tech. Rep. 96–01, Lunar and Planet. Inst., 1996.

Clancy, R. T., and S. W. Lee, A new look at dust and clouds in the Mars atmosphere—Analysis of emission-phase-function sequences from global Viking IRTM observations, *Icarus*, *93*, 135–158, 1991.

Clancy, R. T., A. W. Grossman, M. J. Wolff, P. B. James, D. J. Rudy, Y. N. Billawala, B. J. Sandor, S. W. Lee, and D. O. Muhleman, Water vapor saturation at low altitudes around Mars aphelion: A key to Mars climate?, *Icarus*, *122*, 36–62, 1996.

Clancy, R. T., B. J. Sandor, M. J. Wolff, P. R. Christensen, M. D. Smith, J. C. Pearl, B. J. Conrath, and R. J. Wilson, An intercomparison of ground-based millimeter, MGS TES, and Viking atmospheric temperature measurements: Seasonal and interannual variability of temperatures and dust loading in the global Mars atmosphere, *J. Geophys. Res.*, *105*, 9553–9571, 2000.

Conrath, B. J., Thermal structure of the martian atmosphere during the dissipation of the dust storm of 1971, *Icarus*, *24*, 36–46, 1975.

Davies, D. W., The Mars water cycle, *Icarus*, *45*, 398–414, 1981.

Fanale, F. P., and W. A. Cannon, Exchange of adsorbed H_2O and CO_2 between the regolith and atmosphere of Mars caused by changes in surface insolation, *J. Geophys. Res.*, *79*, 3397–3402, 1974.

Farmer, C. B., D. W. Davies, A. L. Holland, D. D. LaPorte, and P. E. Doms, Mars: Water vapor observations from the Viking Orbiters, *J. Geophys. Res.*, *82*, 4225–4248, 1977.

Fenton, L. K., and M. I. Richardson, Martian surface winds: Insensitivity to orbital changes and implications for aeolian processes, *J. Geophys. Res.*, *106*(E12), 32,885–32,902, 2001.

Forget, F., et al., Improved general circulation models of the Martian atmosphere from the surface to above 80 km, *J. Geophys. Res.*, *104*, 24,155–24,175, 1999.

Goff, J. A., and S. Gratch, Low-pressure properties of water from −160 to 212 F, *Trans. Am. Soc. Heat. Vent. Eng.*, *52*, 95–121, 1946.

Goody, R. M., and M. J. S. Belton, Radiative relaxation times for Mars, *Planet. Space Sci.*, *15*, 247–256, 1967.

Haberle, R. M., and B. M. Jakosky, Sublimation and transport of water from the north residual polar cap on Mars, *J. Geophys. Res.*, *95*, 1423–1437, 1990.

Haberle, R. M., C. B. Leovy, and J. B. Pollack, Some effects of global dust storms on the atmospheric circulation of Mars, *Icarus*, *50*, 322–367, 1982.

Haberle, R. M., J. B. Pollack, J. R. Barnes, R. W. Zurek, C. B. Leovy, J. R. Murphy, H. Lee, and J. Schaeffer, Mars atmospheric dynamics as simulated by the NASA Ames general circulation model, 1, The zonal-mean circulation, *J. Geophys. Res.*, *98*, 3093–3123, 1993.

Hamilton, K., R. J. Wilson, J. D. Mahlman, and L. J. Umscheid, Climatology of the SKYHI troposphere-stratosphere-mesosphere general-circulation model, *J. Atmos. Sci.*, *52*, 5–43, 1995.

Hess, S. L., R. M. Henry, and J. E. Tillman, The seasonal variation of atmospheric pressure on Mars as affected by the south polar cap, *J. Geophys. Res.*, *84*, 2923–2927, 1979.

Holton, J. R., *An Introduction to Dynamic Meteorology*, 2nd ed., Academic, San Diego, Calif., 1992.

Houben, H., R. M. Haberle, R. E. Young, and A. P. Zent, Modeling the Martian seasonal water cycle, *J. Geophys. Res.*, *102*, 9069–9084, 1997.

Houghton, J. T., The absorption of solar infra-red radiation by the lower statosphere, *Q. J. R. Meteorol. Soc.*, *89*, 319–331, 1963.

Ingersoll, A. P., Mars: Occurrence of liquid water, *Science*, *168*, 972–973, 1970.

Jakosky, B. M., The role of seasonal reservoirs in the Mars water cycle, I, Seasonal exchange of water with the regolith, *Icarus*, *55*, 1–18, 1983a.

Jakosky, B. M., The role of seasonal reservoirs in the Mars water cycle, II, Coupled models of the regolith, the polar caps, and atmospheric transport, *Icarus*, *55*, 19–39, 1983b.

Jakosky, B. M., The seasonal cycle of water on Mars, *Space Sci. Rev.*, *41*, 131–200, 1985.

Jakosky, B. M., and E. S. Barker, Comparison of ground-based and Viking Orbiter measurements of Martian water vapor: Variability of the seasonal cycle, *Icarus*, *57*, 322–334, 1984.

Jakosky, B. M., and M. H. Carr, Possible precipitation of ice at low latitudes of Mars during periods of high obliquity, *Nature*, *315*, 559–561, 1985.

Jakosky, B. M., and C. B. Farmer, The seasonal and global behavior of water vapor in the Mars atmosphere: Complete global results of the Viking atmospheric water detector experiment, *J. Geophys. Res.*, *87*, 2999–3019, 1982.

Jakosky, B. M., and R. M. Haberle, The seasonal behavior of water on Mars, in *Mars*, edited by H. H. Kieffer et al., pp. 969–1016, Univ. of Ariz. Press, Tucson, 1992.

James, P. B., The Martian hydrologic cycle: Effects of CO_2 mass flux on global water distribution, *Icarus*, *64*, 249–264, 1985.

James, P. B., and G. R. North, The seasonal CO_2 cycle on Mars: An application of an energy-balance climate model, *J. Geophys. Res.*, *87*(12), 271–283, 1982.

James, P. B., H. H. Kieffer, and D. A. Paige, The seasonal cycle of carbon dioxide on Mars, in *Mars*, edited by H. H. Kieffer et al., pp. 934–968, Univ. of Ariz. Press, Tucson, 1992.

Kieffer, H. H., and A. P. Zent, Quasi-periodic climate change on Mars, in *Mars*, edited by H. H. Kieffer et al., pp. 1180–1218, Univ. of Ariz. Press, Tucson, 1992.

Kieffer, H. H., T. N. Titus, K. F. Mullins, and P. R. Christensen, Mars south polar spring and summer behavior observed by TES: Seasonal cap evolution controlled by frost grain size, *J. Geophys. Res.*, *105*, 9653–9699, 2000.

Mellon, M. T., and B. M. Jakosky, Geographic variations in the thermal and diffusive stability of ground ice on Mars, *J. Geophys. Res.*, *98*, 3345–3364, 1993.

Pearl, J. C., M. D. Smith, B. J. Conrath, J. L. Bandfield, and P. R. Christensen, Observations of Martian ice clouds by the Mars Global Surveyor Thermal Emission Spectrometer, *J. Geophys. Res.*, *106*, 12,325–12,338, 2001.

Richardson, M. I., Comparison of microwave and infrared measurements of martian atmospheric temperatures: Implications for short-term climate variability, *J. Geophys. Res.*, *103*, 5911–5918, 1998.

Richardson, M. I., A general circulation model study of the Mars water cycle, Ph.D. thesis, Univ. of Calif., Los Angeles, 1999.

Richardson, M. I., and R. J. Wilson, Changes in the Martian circulation and climate in response to orbital parameter variations, *Bull. Am. Astron. Soc.*, *32*, 1092, 2000.

Richardson, M. I., and R. J. Wilson, A topographically forced asymmetry in the Martian circulation and climate, *Nature*, *416*, 298–301, 2002.

Richardson, M. I., R. J. Wilson, and A. V. Rodin, Water ice clouds in the Martian atmosphere: General Circulation Model experiments with a simple cloud scheme, *J. Geophys. Res.*, *107*, 10.1029/2001JE001804, in press, 2002.

Smith, D. E., and M. T. Zuber, The shape of Mars and the topographic signature of the hemispheric dichotomy, *Science*, *271*, 184–188, 1996.

Smith, D. E., et al., The global topography of Mars and implications for surface evolution, *Science*, *284*, 1495–1503, 1999.

Smith M., Annual cycle of water vapor on Mars as observed by the Thermal Emission Spectrometer, *J. Geophys. Res.*, *107*, 10.1029/2001JE001522, in press, 2002.

Sprague, A. L., D. M. Hunten, R. E. Hill, B. Rizk, and W. K. Wells, Martian water vapor, 1988–1995, *J. Geophys. Res.*, *101*, 23,229–23,241, 1996.

Stull, R. B., *An Introduction to Boundary Layer Meteorology*, Kluwer Acad., Norwell, Mass., 1988.

Tamppari, L. K., R. W. Zurek, and D. A. Paige, Viking era water-ice clouds, *J. Geophys. Res.*, *105*, 4087–4107, 2000.

Vasavada, A. R., Surface properties of Mars' polar layered deposits and polar landing sites, *J. Geophys. Res.*, *105*, 6961–6969, 2000.

Wilson, R. J., A general circulation model simulation of the Martian polar warming, *Geophys. Res. Lett.*, *24*, 123–127, 1997.

Wilson, R. J., Evidence for diurnal period Kelvin waves in the Martian atmosphere from Mars Global Surveyor TES data, *Geophys. Res. Lett.*, *27*, 3889–3892, 2000.

Wilson, R. J., and K. P. Hamilton, Comprehensive model simulation of thermal tides in the martian atmosphere, *J. Atmos. Sci.*, *53*, 1290–1326, 1996.

Wilson, R. J., and M. I. Richardson, The Martian atmosphere during the Viking mission, 1, Infrared measurements of atmospheric temperatures revisited, *Icarus*, *145*, 555–579, 2000.

Zent, A. P., and R. C. Quinn, Measurement of H_2O adsorbtion under Mars-like conditions: Effects of adsorbent heterogeneity, *J. Geophys. Res.*, *102*, 9085–9095, 1997.

Zent, A. P., R. M. Haberle, H. C. Houben, and B. M. Jakosky, A coupled subsurface-boundary layer model for water on Mars, *J. Geophys. Res.*, *98*, 3319–3337, 1993.

Zurek, R. W., J. R. Barnes, R. M. Haberle, J. B. Pollack, J. E. Tillman, and C. B. Leovy, Dynamics of the atmosphere of Mars, in *Mars*, edited by H. H. Kieffer et al., pp. 835–933, Univ. of Ariz. Press, Tucson, 1992.

───────────────

M. I. Richardson, Division of Geological and Planetary Sciences, California Institute of Technology, Pasadena, CA 91125, USA. (mir@gps.caltech.edu)

R. J. Wilson, Geophysical Fluid Dynamics Laboratory, National Oceanic and Atmospheric Administration, P.O. Box 308, Princeton, NJ 08542, USA. (rjw@gfdl.gov)

Figure 1. The latitudinal and seasonal distribution of water vapor in the Martian atmosphere, as observed by the Viking Mars Atmospheric Water Detector (MAWD) [*Farmer et al.*, 1977; *Jakosky and Farmer*, 1982]. The data have been zonally averaged and binned by 6° of latitude and 6° of L_s. The contour and color levels are on the same scale, with color intervals at 1, 2, 3, 4, 6, 8, 10, 12, 14, 16, 20, 30, 40, 50, 70, and 90 prµm, and contour levels at 1, 6, 10, 16, 30, 40, and 90 prµm. Data are shown for the first and second years of Viking observations; the third year of data being extremely sparse. The blue horizontal lines in Year 1 (top) roughly indicate the occurrence of two major dust storms that significantly degrade data quality. Despite the dust storms, note the appearance of two maxima in water vapor during southern summer (between the storms, $L_s = 250°-270°$), with one maxima in the high southern latitudes and one in the northern tropics.